CHEMICAL REVIEWS

pubs.acs.org/CR

Review

Nonlinear Phenomena in Microfluidics

Sarah Battat,* David A. Weitz,* and George M. Whitesides*

Cite This: *Chem. Rev.* 2022, 122, 6921−6937

Read Online

ABSTRACT: This review focuses on experimental work on nonlinear phenomena in microfluidics, which for the most part are phenomena for which the velocity of a fluid flowing through a microfluidic channel does not scale proportionately with the pressure drop. Examples include oscillations, flow-switching behaviors, and bifurcations. These phenomena are qualitatively distinct from laminar, diffusion-limited flows that are often associated with microfluidics. We explore the nonlinear behaviors of bubbles or droplets when they travel alone or in trains through a microfluidic network or when they assemble into either one- or two-dimensional crystals. We consider the nonlinearities that can be induced by the geometry of channels, such as their curvature or the bas-relief patterning of their base. By casting posts, barriers, or membranes—situated inside channels—from stimuli-responsive or flexible materials, the shape, size, or configuration of these elements can be altered by flowing fluids, which may enable autonomous flow control. We also highlight some of the nonlinearities that arise from operating devices at intermediate Reynolds numbers or from using non-Newtonian fluids or liquid metals. We include a brief discussion of relevant practical applications, including flow gating, mixing, and particle separations.

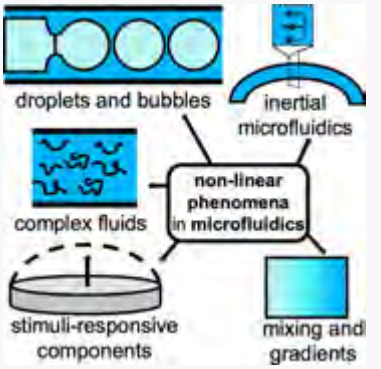

CONTENTS

1. INTRODUCTION

Fluid flows in microfluidic devices usually occur on small scales and at slow speeds. They are laminar, stable to perturbations, and dominated by viscous forces.[1] Generally, the velocity of the fluid scales linearly with the pressure change across the channel.[1,2] Surprisingly, there exists a rich array of nonlinear phenomena that occur in microfluidic devices.[3] These include spontaneous oscillations in the flow rate of fluids,[4,5] sudden

Special Issue: Microfluidics

Received: November 26, 2021
Published: February 23, 2022

https://doi.org/10.1021/acs.chemrev.1c00985
Chem. Rev. 2022, 122, 6921−6937

changes in the operating modes of droplet makers,[6] and instabilities driven by surface tension.[7] In most examples discussed in this review, the flow velocity does *not* scale proportionately with the applied pressure difference. In other examples, a nonlinear scaling exists between different variables, which results in flows that are qualitatively distinct from the usual laminar and time-reversible microfluidic flows.

Microfluidic flows are generally well-described by the Stokes equation, an approximation to the Navier−Stokes equation in the limit of negligible inertial forces. Nonlinearities in the velocity−pressure scaling arise when the physics of a microfluidic system deviates from that captured in the Stokes equation. For instance, in two-phase flows, the shape of a boundary between two phases changes due to deformations induced by the flow; this dependence on the flow, coupled with interfacial tension, gives rise to nonlinearities. Moreover, when bubbles or droplets are positioned sufficiently close together, their positions and hence velocities depend on those of their neighbors, which disturb the flow. This feedback loop, in which the flow dictates the shapes and/or positions of the bubbles or droplets and they in turn disturb the flow, gives rise to nonlinear behavior. Nonlinear boundary conditions also arise when channel walls are deformed by the flow. Inertial, and hence nonlinear, corrections to the Stokes equation must be considered when microchannels are curved or the flow velocity is sufficiently high. These cases, among others, are examples of the breadth of nonlinear phenomena that can occur in microfluidics.

Nonlinear phenomena in microfluidics are interesting to study in their own right. Many of the explanations for the phenomena are counterintuitive and require new ways of thinking about the capabilities of microfluidic flows. This review will explore some of these phenomena with particular emphasis on those that occur in one- and two-phase flows.[8] It combines a treatment of nonlinearities caused by bubbles and droplets with special topics ranging from mixing to capillary-driven flows. It also covers more commonly discussed topics in nonlinear microfluidics including inertial flows, stimuli-responsive materials in microfluidic devices, and non-Newtonian fluids.

First, we will highlight the nonlinearities that arise when single bubbles or droplets traverse microfluidic networks composed of paths that split apart or merge together. To appreciate these behaviors, we will provide a general overview of the methods to produce droplets and bubbles in microfluidic devices. Second, we will consider the behavior of these bubbles or droplets as they move in single-file trains or when they form ordered crystals. Third, we will discuss nonlinearities that arise from the geometric features of channels, the importance of inertial flow effects, the flow of non-Newtonian fluids and liquid metals, and the use of stimuli-responsive materials in fabricating devices. Where relevant, we will highlight possible applications of nonlinear flows in microfluidics, ranging from particle filtration[9,10] to autonomous flow control.[11,12]

2. OVERVIEW OF BUBBLE AND DROPLET GENERATION IN MICROFLUIDIC DEVICES

Microfluidics makes it possible to manipulate fluids precisely at the micron scale.[13] This control enables micrometer-sized bubbles or droplets to be produced by dispersing a gas or a liquid into an immiscible liquid phase. Their volume, dispersity in size, and packing density can be tuned depending on the geometry of the microfluidic device and the flow regime in which it is operated, among other parameters. Bubbles and droplets are formed through nonlinear processes, given the instabilities that lead to their formation and the effects of surface tension.[7,14−16] Thus, an overview of the production of bubbles or droplets is a prerequisite to understanding their nonlinear behaviors in microfluidic networks. Although bubbles and droplets will be discussed side-by-side, some of their notable differences include their density, viscosity, and compressibility under large applied pressures.

2.1. Dimensionless Parameters

Most fluid flows in microfluidic devices occur at low Reynolds numbers. The Reynolds number, Re, is a dimensionless parameter that describes the ratio of inertial forces ($\rho u^2/l$) to viscous forces ($\mu u/l^2$) acting on a volume element of a fluid (eq 1):

$$Re = \frac{\rho u l}{\mu} \tag{1}$$

where ρ is the density of the fluid, μ is the dynamic viscosity of the fluid, u is the characteristic velocity of the fluid, and l is the most relevant length scale in the device.[17,7,2] The Stokes equation, given in eq 2, approximates the Navier−Stokes equation in the limit of low Reynolds numbers for incompressible, single-phase Newtonian fluids:

$$0 = -\nabla p + \mu \nabla^2 \boldsymbol{U} \tag{2}$$

where p is the pressure, μ is the dynamic viscosity of the fluid, and $\boldsymbol{U}$ is the velocity field. Its solutions are linear and time-reversible so long as the channel geometry is fixed.[1,2,18] The condition of the conservation of mass of an incompressible fluid is given by the continuity equation:

$$\nabla \cdot \boldsymbol{U} = 0 \tag{3}$$

.[1,2,18] Table 1 highlights other dimensionless parameters[17,7,19,20] that quantify the relative influence of forces on the flow behavior, especially in two-phase flows where surface tension becomes important.

Table 1. Dimensionless Parameters of Relevance in Microfluidics

capillary number	$Ca = \frac{\mu u}{\gamma}$	ratio of viscous to interfacial tension forces
Weber number	$We = \frac{\rho u^2 l}{\gamma}$	ratio of inertial to interfacial tension forces
Ohnesorge number	$Oh = \frac{\mu}{\sqrt{\rho l \gamma}}$	ratio of viscous to inertial and interfacial tension forces
Bond number	$Bo = \frac{\rho g l^2}{\gamma}$	ratio of gravitational to interfacial tension forces
Peclet number	$Pe = \frac{ul}{D}$	ratio of convective to diffusive transport speeds

where		
	μ: dynamic viscosity of the fluid	SI units: $Pa{\cdot}s$
	ρ: density of the fluid	SI units: $kg{\cdot}m^{-3}$
	γ: interfacial tension	SI units: $N{\cdot}m^{-1}$
	u: characteristic velocity of the fluid	SI units: $m{\cdot}s^{-1}$
	l: characteristic length scale	SI units: m
	g gravitational acceleration	SI units: $m{\cdot}s^{-2}$
	D: diffusion coefficient	SI units: $m^2{\cdot}s^{-1}$

https://doi.org/10.1021/acs.chemrev.1c00985
Chem. Rev. 2022, 122, 6921−6937

2.2. Methods of Production for Bubbles and Droplets

Micrometer-sized droplets or bubbles can be produced using a variety of microfluidic devices, as illustrated schematically in Figure 1. Although the dispersed (or inner) phase is always injected into the continuous (or outer) phase, the devices differ in the way in which the two phases meet. In a *co-flowing device*, the dispersed phase is injected through a micrometer-sized orifice into a flowing parallel stream of the continuous phase, as depicted in Figure 1a. In a *flow-focusing geometry*, the dispersed phase is also injected into a co-flowing stream of the continuous phase; however, an aperture beyond the injection nozzle further constrains and accelerates the inner phase, as shown in Figure 1b. In a *T-junction geometry*, the immiscible phases are injected into two different channels that meet at a right angle, as shown in Figure 1c.[7,14−16] Bubbles and droplets can be produced in other manners beyond those discussed here. For instance, *step emulsification* is a method by which the dispersed and continuous phases are co-flowed or meet at a T-junction, but the droplet or bubble breakup only occurs when the height of the device changes abruptly, namely beyond a *step*.[21−23] Generally, the details of the bubble or droplet production depend on the relative magnitude of viscous, inertial, and interfacial tension forces. Bubbles or droplets that are generated in microfluidic devices are typically the same order of magnitude in size as the channel or orifice in or from which they are produced.[7]

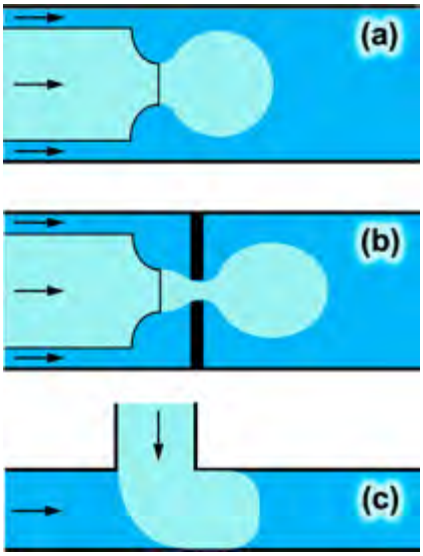

Figure 1. Production of bubbles or droplets in (a) co-flowing, (b) flow-focusing, and (c) T-junction microfluidic geometries, where the continuous phase is depicted in dark blue, the dispersed phase is drawn in light blue, and the flow directions are specified by arrows.

2.2.1. Production of Droplets or Bubbles at Low Capillary Numbers (Ca < 10^{-2}). In co-flowing devices, droplets are produced in the *dripping mode* when both the Weber number of the dispersed phase and the capillary number of the continuous phase are below or of $O(1)$ (where O denotes the order of magnitude and the numbers enclosed in the parentheses indicate the order of magnitude).[24−26] In the dripping mode, surface tension holds a growing droplet in place at the orifice, and the droplet is released when the viscous drag exceeds the surface tension. Droplets that are generated by dripping are uniform in size. When the Weber number of the dispersed phase exceeds $O(1)$, despite low values of the capillary number of the continuous phase, a qualitatively distinct mode of droplet production is observed. Given the inertia of the inner phase at such Weber numbers, a short jet forms; it widens, and the droplet detaches at its end.[24] The dripping regime has also been reported when bubbles are formed in co-flowing devices, but the mechanism depends on the pressure of the gas phase as well as the flow rate and viscosity of the continuous phase.[27,28]

In the flow-focusing[29−31] and planar T-junction[32−34] geometries, confinement plays a crucial role in the formation of droplets and bubbles. For instance, when operating a flow-focusing device at capillary numbers of the continuous phase below $O(10^{-1})$, the dispersed phase forms a thread that narrows in the aperture—this part is subsequently referred to as the *neck*—and widens once past it. As the droplet or bubble

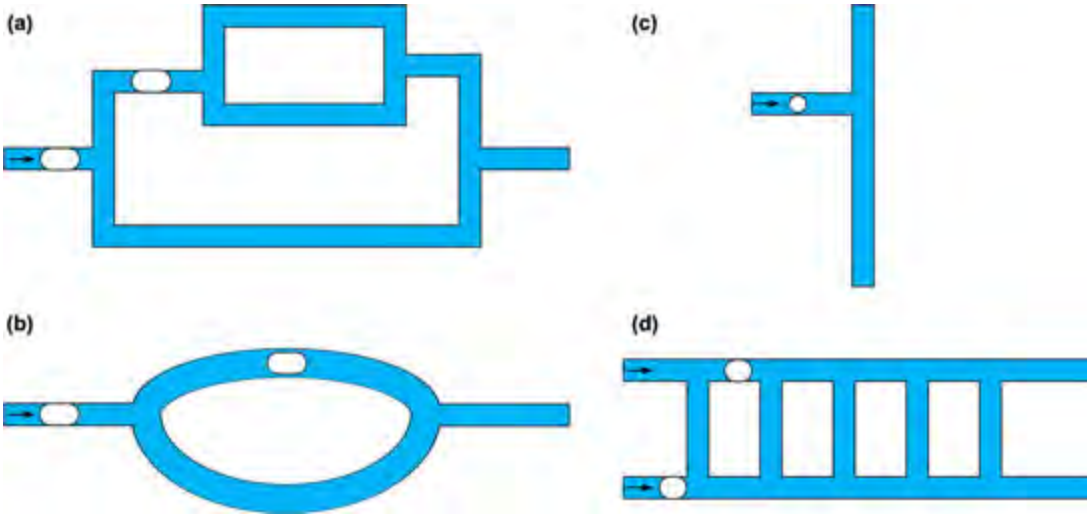

Figure 2. Movement of bubbles or droplets, drawn in white, through a liquid, depicted in blue, in (a) a microfluidic network composed of cascaded T-junctions, (b) an asymmetric closed loop with branches of different lengths, (c) a T-junction network that splits into two branches of different lengths, and (d) a ladder-inspired microfluidic device that synchronizes bubbles. The flow direction of the liquid is specified by arrows, and the cross-sectional areas of the channels are constant.

https://doi.org/10.1021/acs.chemrev.1c00985
Chem. Rev. 2022, 122, 6921−6937

grows, it blocks the flow of the continuous phase, which causes an increase in pressure further upstream. The continuous phase squeezes the neck of the immiscible thread, hence the designation of *squeezing regime*. Eventually, the neck collapses when it becomes sufficiently thin, and a bubble or droplet is released.[29,35] The measured speed of the collapse of the neck is independent of surface tension and orders of magnitude slower than that of the capillary instabilities propagating along the thread. The thread transitions through a series of equilibrium states, each of which is defined as the shape with minimum surface energy that encloses the dispensed volume of the dispersed phase, before it ultimately breaks at the neck in a reproducible manner.[36,35] The same squeezing mechanism occurs in T-junction devices.[32,33,37]

2.2.2. Production of Droplets or Bubbles at High Capillary Numbers (Ca > 10^{-1}). When co-flowing two immiscible liquids, *jetting* is observed for Ca = $O(10^{-1}-10^{0})$ irrespective of the Weber number of the dispersed phase. The viscous shear stresses cause the dispersed phase to form a thinning jet. The jet breaks up into droplets due to the growth and propagation of Rayleigh−Plateau instabilities along its length.[24] A *Rayleigh−Plateau instability* propagates as a wave on a cylindrical fluid jet and ultimately results in the breakup of the jet into drops to minimize surface area.[38]

In T-junction geometries, for example, at capillary numbers of $O(10^{-1})$ the thread of the dispersed phase is longer and thinner than that in the squeezing regime. Droplet breakup occurs further from the junction where the dispersed and continuous phases meet. Evidence of squeezing, however, remains. Low-amplitude pressure oscillations in the continuous phase are observed, and the dips in pressure coincide with the release of a droplet. When the capillary number increases even more, jetting occurs, and a long, thin thread of the dispersed phase extends into the channel through which the continuous phase flows.[33,37,34] Jetting has also been observed in flow-focusing geometries.[30]

3. INDIVIDUAL BUBBLES OR DROPLETS IN MICROFLUIDIC NETWORKS

As bubbles or droplets travel through microfluidic networks composed of channels with constant cross-sectional areas, such as those depicted in Figure 2, they show nonlinear behaviors. At a junction of two diverging paths, a bubble or droplet will choose the path with the lower hydraulic resistance or, equivalently, the one through which the continuous phase flows more quickly.[39−41] The hydraulic resistance is a measure of how difficult it is for a fluid to flow through a channel; it is defined as the ratio between the pressure difference across the channel and the resultant flow rate.[18] The decision of which path to select is *local* because it depends on the flow rates of the continuous phase through the branches immediately extending from the junction. The flow rates are, of course, dependent on the configuration of bubbles or droplets throughout the network at any given time; the presence of other bubbles or droplets within the network will dynamically alter the resistance of each branch. Therefore, the overall path that a bubble or droplet takes—from its entry into to its exit from a network—may not be the shortest one in distance.[39] The discussion here will focus on bubbles or droplets that do not split at junctions and whose inter-droplet spacing, λ, is large as compared to their size.

The path selected by a droplet entering a microfluidic network depends on the hydraulic resistance of the network devoid of droplets and the presence of other droplets within the network. An asymmetric closed loop, for instance, consists of two branches of different lengths that diverge at a junction and rejoin at the outlet, as depicted in Figure 2b. In the absence of other droplets in the loop, an incoming droplet will travel through the shorter branch because it has a lower hydraulic resistance than the longer one. Nevertheless, should a droplet already be present in the shorter branch as another droplet enters the loop, the hydraulic resistance of the shorter branch will be greater than in its empty state.[6] Therefore, the hydraulic resistance of any branch, R_i, varies in time and can be expressed as eq 4:

$$R_i(t) = \bar{R}_i + n_i(t)R_d \tag{4}$$

where $\bar{R}_i$ is the resistance of the branch in the absence of droplets, $n_i(t)$ is the number of droplets residing in the branch at any given time, and R_d is the contribution of an individual droplet to the hydraulic resistance.[42] In the asymmetric closed loop, water-in-oil droplets are produced at regularly spaced time intervals. They admit nonlinear behaviors: the time intervals between consecutive droplets that emerge from the closed loop may differ from those between droplets that enter it. As droplets are produced more frequently, more reside in the network at any given moment in time and the resistance of each branch deviates from its original value of $\bar{R}_i$ in accordance with eq 4.[42,6,43] Period-n and aperiodic behaviors have both been observed. Period-n, where $n = \{1, 2, 3, 4, 5, 7\}$, refers to the n distinct time intervals between droplets that emerge consecutively from a network. These time intervals repeat, which means that the time interval between the first and second droplet is the same as that between the $(n + 1)^{th}$ and the $(n + 2)^{th}$ droplet. The system moves from different period-n to aperiodic modes as the frequency of droplet generation is altered. Despite these obvious nonlinearities, time-reversibility is preserved: the original, regularly spaced time intervals between incoming droplets can be recovered by running the flow in reverse.[6]

The nonlinear behavior of individual bubbles and droplets in networks could perhaps be used to manipulate droplets in microfluidic devices. For instance, a ladder-inspired device composed of two separate parallel channels that are connected by a series of transverse channels, or *rungs* on a ladder, synchronizes the motion of two bubbles that enter the ladder through separate parallel channels at different times, as pictured in Figure 2d.[44,45] When the continuous phase flows through the parallel channels at the same flow rate and the channel outlets are maintained at a constant pressure, the leading bubble will slow and emerge from the device at approximately the same time as the lagging bubble.[42] This phenomenon occurs due to a flow induced from the channel containing the leading bubble to that holding the lagging one.[44] Given the asymmetry in the boundary conditions, the lag between the two bubbles can be re-established by operating the device in reverse.[42] The presence of a surfactant in the continuous phase could potentially affect the velocity of the bubbles, as was demonstrated for the case of bubbles flowing through two identical branches that split at a junction and merge further downstream.[46] The synchronization of bubbles or droplets could be important when, for example, merging bubbles or droplets produced in separate bubble or droplet makers.

https://doi.org/10.1021/acs.chemrev.1c00985
Chem. Rev. 2022, 122, 6921−6937

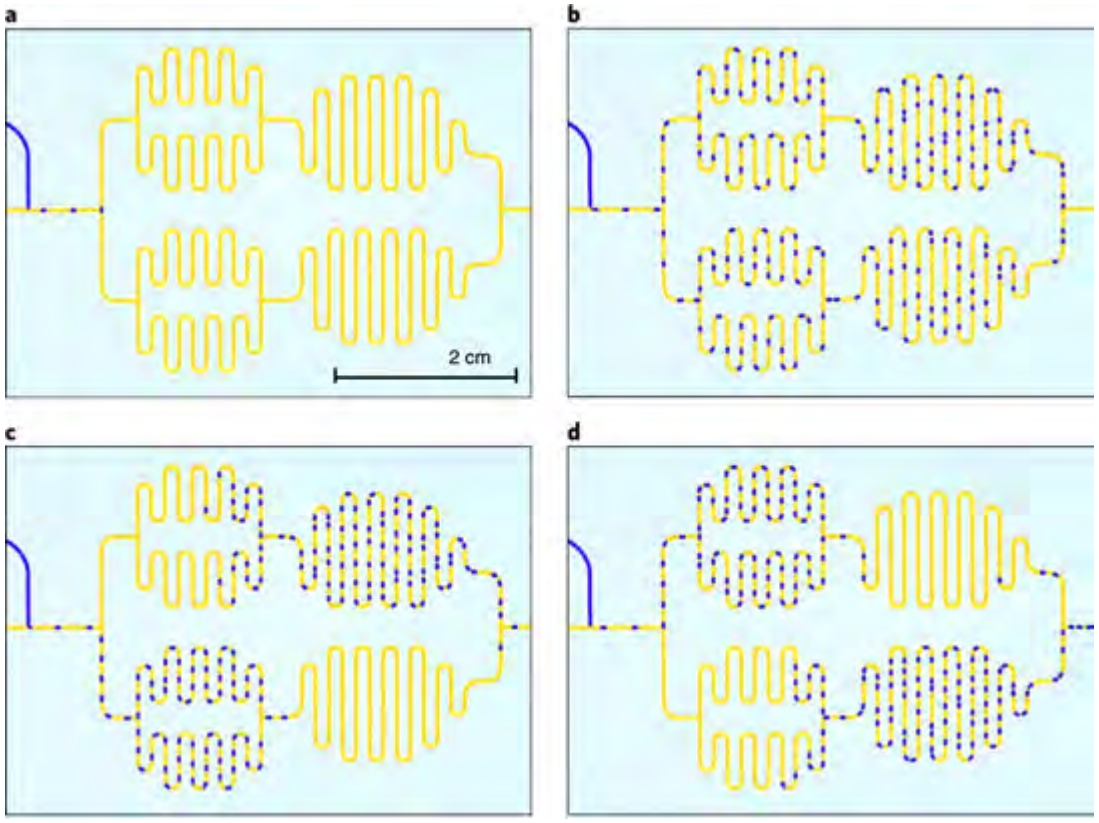

Figure 3. Water droplets (blue) flowing in oil (yellow) initially distribute themselves along all branches of a microfluidic network (a and b), but eventually organize into trains that oscillate between branches (c and d). Figure reproduced from 49. Copyright 2019 Springer Nature.

4. BUBBLE OR DROPLET TRAINS IN MICROFLUIDIC NETWORKS

Trains of bubbles or droplets refer to a sequence of closely spaced bubbles or droplets, separated by a constant distance, λ. The behavior of trains of bubbles or droplets in microfluidic networks is qualitatively different from that of individual bubbles or droplets. For instance, in a network composed of cascaded T-junctions such as that shown in Figure 2a, this shift in behavior occurs at a critical number density, namely when the total hydraulic resistance contributed by all the bubbles in the network is approximately equal to the hydraulic resistance of a path—devoid of bubbles but containing the continuous phase—connecting the inlet and outlet of the network.[39] Leading droplets in the train interact with branches beyond the junction and report *global information* on the network through changes in the flow rate and pressure. The bubbles in the train behave like the continuous phase, distributing themselves among the different paths in roughly the same ratio as that for the flow rate of the continuous phase. As such, most bubbles follow the path in which the carrier fluid moves most quickly, namely the shortest path in the network.[39,47]

4.1. Collective Hydrodynamic Feedback and Collisions of Bubbles or Droplets

When bubbles and droplets move in trains, their spacing and confinement impacts the way in which they interact.[39,40] For instance, as shown in Figure 2c, when a train of monodisperse water-in-oil droplets arrives at a T-junction that splits into two branches of different lengths, each of which terminates at separate outlets maintained at the same pressure, the droplets divide between both branches.[40,48] The mechanism that drives their repartition (namely their separation between branches), however, depends on the extent of their confinement. The confinement is quantified by the ratio, ρ_c, of the radius of the droplet to that of the channel. As expected, when droplets are small and sufficiently far apart to not qualify as entities in a train, they travel through the shorter branch and hardly add to the hydrodynamic resistance of the channels. Below a critical value of the inter-droplet spacing, λ, however, droplets in a train will be diverted to the longer branch because the hydrodynamic resistance of the shorter branch when filled with droplets exceeds that of the longer branch. Keeping the inter-droplet spacing constant, repartition of droplets into both branches occurs due to either collective hydrodynamic feedback when $\rho_c > 0.85$ or collisions when $\rho_c < 0.75$.[40]

Phenomena in vehicular traffic[11] and the circulation of red blood cells (RBCs)[49,50] have also been observed in microfluidic networks filled with bubble or droplet trains. For instance, in a microfluidic vascular network composed of serpentine channels that split and join at T-junctions, confined water-in-oil droplets initially explore all paths;[40] eventually, however, they organize into trains that oscillate between the branches.[49] This phenomenon is illustrated in Figure 3. These oscillations can be suppressed by inter-droplet collisions at junctions and thus through momentary changes in the frequency of droplet production. The simultaneous occurrence of oscillations and collisions could explain why low-amplitude oscillations of RBCs in vascular networks have been observed in animals and humans.[51,52] Nevertheless, the collision of RBCs is a less deterministic process than that of droplets, as a successful collision of RBCs requires two properly oriented RBCs to reside in a junction at a given time. A model of the

https://doi.org/10.1021/acs.chemrev.1c00985
Chem. Rev. 2022, 122, 6921−6937

droplets in the microfluidic network, which accounts for probabilistic droplet collisions by way of the plasma skimming function (eq 5) and omits details of the flow around each droplet, predicts small amplitude oscillations in certain conditions. The plasma skimming function is given by eq 5:

$$p(Q_i) = \frac{Q_i^{\,s}}{Q_i^{\,s} + Q_j^{\,s}} \tag{5}$$

where the subscripts i and j refer to two separate branches beyond a junction, Q is the flow rate in either branch, and s is an exponent that reflects the degree of determinism in the system. In the limit of $s \to \infty$, the system is deterministic, and the droplets will always travel through the branch in which the continuous phase flows the fastest. When $s = 1$, the probability that a droplet travels through a certain branch is proportional to the flow rate therein. Mathematical models based on actual *in vitro* data estimate $s = 2-2.5$, while continuous hemodynamic models overestimate the parameter at values of $s > 4$ or $s > 5$. The microfluidic model estimates $s = 2.2$, in close agreement with the values based on *in vitro* measurements.[49]

The size and spatial arrangement of bubbles and droplets in a train can be made more complex beyond a single-file line of monodisperse bubbles and droplets. For instance, droplets can assume complex spatial patterns and shapes in the outlet of a T-junction device;[34,53] similarly, bubbles or droplets can assume intricate arrangements in an outlet shared by several flow-focusing devices.[54] It is also possible to generate a stable periodic train of multidisperse bubbles in a modified T-junction device operated at intermediate pressures, whereby five T-junctions are cascaded and all channels carrying the continuous phase are connected (Figure 4). The breakup of the gaseous thread into a periodic collection of bubbles occurs due to a separation of timescales, namely the slower timescale of the breakup of the gaseous thread and the faster one describing the transmission of pressure among the T-junction nodes at the speed of sound in water. This periodic behavior is resilient for nearly 10^5 periods.[55] In flow-focusing devices, periodic and chaotic bubbling modes have also been reported at capillary numbers of $O(10^{-4}-10^{-2})$ and Reynolds numbers as high as $O(10^2)$. Monodisperse, period-2, period-3, and period-4 modes have been achieved, where period-n refers to the n number of sizes of bubbles that are produced iteratively. Inertial effects and the recoil of the gaseous thread after breakup are predominantly responsible for such bifurcations in the size periodicity.[56] Flow-focusing devices that are coupled, meaning that adjacent devices share their supply of the continuous phase but have their own inlet for the dispersed phase, can also be used to produce period-1, period-2, and period-4 bubble trains.[57]

5. MICROFLUIDIC CRYSTALS

5.1. One-Dimensional Microfluidic Crystals

A one-dimensional (1D) microfluidic crystal can be defined as a train of evenly spaced, pancake-shaped droplets, or equivalently bubbles, that flows through a channel.[58] The droplets are wedged between the top and bottom walls of a channel and may or may not contact the lateral walls of the channel depending on their volume. They experience drag forces, due to the flow of the continuous phase and the hydrodynamic interactions with neighboring droplets, and

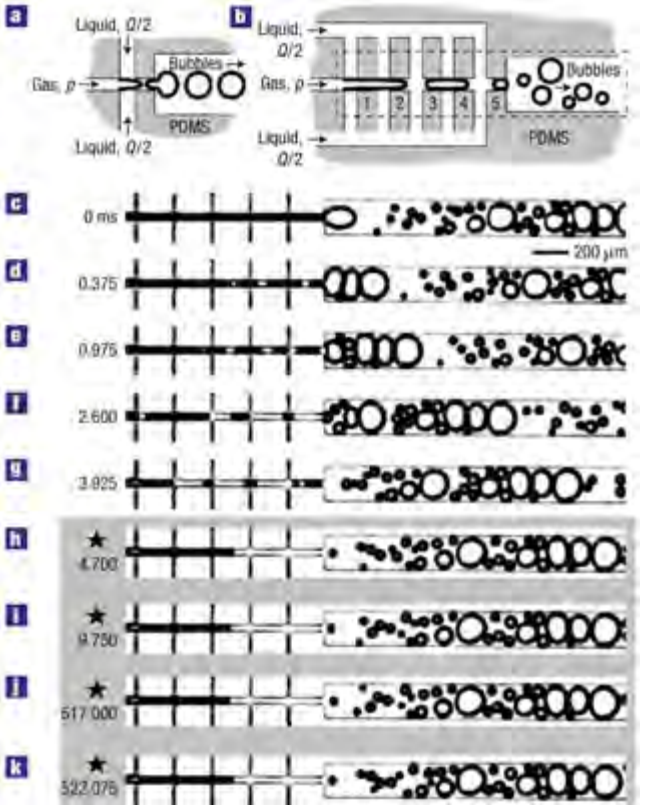

Figure 4. (b) Generation of periodic bubble trains in a modified microfluidic T-junction device, as compared to the traditional device depicted in (a), composed of five T-junctions placed in series, (c–g) pictured at five different moments during a single period and (h–k) at four later times for which the same pattern can be observed. Figure reproduced from 55. Copyright 2005 Springer Nature.

frictional forces due to their contact with the channel walls. The drag and frictional forces should sum to zero given the low Reynolds number condition. The dipolar hydrodynamic force between droplet pairs decays as $1/r^2$, where r is the radial distance from the droplet. The force increases as the inter-droplet spacing decreases and is directed opposite to the flow. Thus, a group of droplets whose inter-droplet spacing is smaller than that characteristic of the rest of the crystal will move more slowly. The droplets moving behind this group will catch up to it, while those ahead of it will escape. Consequently, the densely packed group of droplets will move opposite to the continuous phase with a characteristic longitudinal wave speed, as depicted in Figure 5. Moreover, in the reference frame of the continuous phase, the crystal will appear to move more quickly as the inter-droplet spacing decreases.[59,58]

A 1D microfluidic crystal exhibits transverse (in y) and longitudinal (in x) excitation modes that are analogous to phonon modes in solid-state crystals and that depend on the geometric confinement of the droplets or bubbles. Out-of-plane vibrational modes are not allowed because the crystal is wedged between the top and bottom walls of the channel.[58] The confinement parameter, γ_c, is the ratio of the droplet diameter to the width of the channel. For unconfined droplets with $\gamma_c \leq 0.1$, the dispersion relations, $\omega(k)$, that give the angular frequency of the waves, ω, as a function of their wavenumber, k, are antisymmetric: $\omega_x(k) = -\omega_y(k)$. In contrast to the symmetry of standing waves accommodated

https://doi.org/10.1021/acs.chemrev.1c00985
Chem. Rev. 2022, 122, 6921–6937

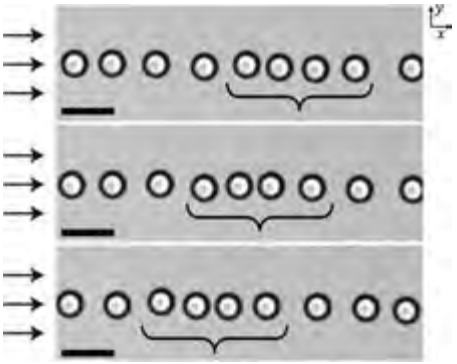

Figure 5. Longitudinal wave traveling through a one-dimensional microfluidic crystal composed of water-in-oil droplets. The droplets touch the top and bottom walls of the microfluidic channel, and the direction of the flow of the oil is specified by the arrows (scale bar: 50 μm). Figure adapted from 58. Copyright 2006 Springer Nature.

in most harmonic crystals, this antisymmetric property arises due to the unidirectional flow of the continuous phase. Defects in the crystal can be attributed to the finite length or perturbation of the droplet train. When droplets are confined, the crystal exhibits qualitatively different behaviors. In particular, the longitudinal and transverse wave modes are no longer antisymmetric. Vibrational modes cannot be detected when $\gamma_c \gtrsim 0.65$, as the droplets impede the flow of the continuous phase so significantly that excitation modes cannot be induced.[59,60]

In an ensemble of microfluidic droplets that randomly occupy and flow through a two-dimensional space, long-range velocity correlations exist due to hydrodynamic interactions.[59,61,62] These correlations can be reproduced in a model that accounts for the hydrodynamic interactions between a dipole pair and a third droplet, representing the ensemble.[61]

5.2. Two-Dimensional Microfluidic Crystals

Two-dimensional (2D) microfluidic crystals are packings of monodisperse bubbles or droplets that exhibit spatial ordering and form a monolayer due to confinement between the top and bottom walls of a microfluidic channel.[63] For slow-flowing crystals, preferred packing structures tend to minimize interfacial energy. The structures depend on parameters such as the volume fraction (or projected surface area coverage) of the dispersed phase, the cross-sectional area of the bubbles or droplets, and the width of the channel containing the crystal.[63−65] Some structures are unstable and can change in time due to topological rearrangements. For example, as shown in Figure 6a, a 2D microfluidic crystal produced in a flow-focusing device can coexist in two states: a hex-two structure, composed of two rows of closely packed bubbles, and a hex-one structure, composed of one row of bubbles that all span the width of the channel.[66,67] This coexistence occurs over a certain range of pressures of the gas phase.[67] Surprisingly, the flow velocity of the crystal does not change over this range, and the front that demarcates the transition between the hex-one and hex-two structures remains stationary.[67,68] Oscillatory or entirely random transitions between the hex-one and hex-two structures can also be induced.[67]

5.2.1. Topological Rearrangements. In many instances, the topological rearrangements that are responsible for this kind of structure switching[67] are classified as *T1 events*.[69] T1 events correspond to the rearrangement of four adjacent droplets or bubbles to reduce the total interfacial energy,[69] as depicted schematically in Figure 6b. Two of the bubbles or droplets, referred to as the diverging pair, are initially touching one another, while the other two, referred to as the converging pair, are vertically separated by the diverging pair. The pairs rearrange such that the converging pair ultimately touches and the diverging pair is separated horizontally by the converging pair.[70,71] T1 events propagate in a specific direction at a characteristic wave velocity.[70−72] They have been observed as a 2D hexagonal crystal composed of oil droplets flows through a linearly tapered constriction[70,71] or as a dense packing of bubbles flows through a channel with constrictions and expansions.[72] These events are localized spatially to specific areas of the channel, termed *rearrangement zones*.[70−72]

6. NONLINEAR FLOWS IN MICROFLUIDIC DEVICES

6.1. Mixing

Mixing is a process characteristic of high-Reynolds-number, turbulent flows. The process of mixing two liquids together is diffusion-limited at low Peclet numbers. To compensate, prohibitively long channels are required for adequate mixing to occur. This challenge can be overcome by the bas-relief patterning of an asymmetric herringbone motif on the floor of a microfluidic device, which induces rotational and extensional flows. The ridges generate transverse components in the flow because the fluid encounters less viscous resistance moving along the ridges than moving orthogonal to them. By alternating the orientation of and tuning the degree of asymmetry of the herringbones, the center of rotation of the fluids and the mixing efficiency, respectively, can be changed, as shown in Figure 7. In the staggered herringbone design, the mixing length is shortened, growing as the logarithm of the Peclet number rather than linearly with the Peclet number as in the laminar flow regime.[73] Although the flow velocity scales linearly with the pressure drop across the channel, the three-dimensionality of the flow leads to flow characteristics unexpected for Re < 100. Moreover, the mixing problem itself

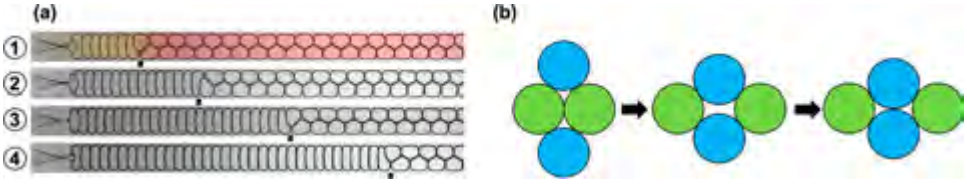

Figure 6. (a) Coexistence of hex-one (shaded in yellow) and hex-two (shaded in red) phases, where the continuous phase flows at 5 μL·min^{-1} and the pressure of the gas phase is 3.46, 3.75, 4.09, and 4.73 kPa (from the top to bottom panels). The position of the stationary front where the structure switching occurs is denoted by the black dot. (b) Schematic illustration of a T1 rearrangement event of droplets or bubbles, where the converging pair is in blue and the diverging pair is in green. Panel (a) adapted from 67. Copyright 2009 American Physical Society.

https://doi.org/10.1021/acs.chemrev.1c00985
Chem. Rev. 2022, 122, 6921−6937

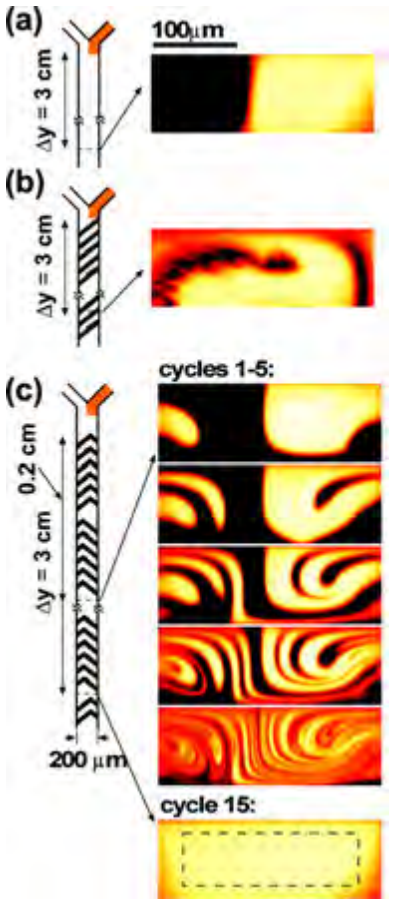

Figure 7. Flow of two miscible solutions, one labeled with fluorescein, at Re ~ $O(10^{-2})$ through a channel (a) without patterning, (b) with ridges on its floor, or (c) with a staggered herringbone motif on its floor. The flow is imaged at (a and b) 3 cm and (c) 0.2, 0.4, 0.6, 0.8, 1, and 3 cm from the injection point. Figure adapted from 73. Reprinted with permission from AAAS. Copyright 2002 AAAS.

is nonlinear. If one were to track the position of a dyed fluid element, the position of the fluid element would depend on the three-dimensionality of the flow, thereby resulting in a complex nonlinear function. Mixing can be achieved through other methods in microfluidics,[74,75] ranging from oscillatory flow perturbations[76] to bubbles or droplets as fluid mixers or containers for mixing.[77,78]

6.2. Gradient Makers

Controlled concentration gradients are difficult to generate in microfluidic devices due to diffusion-limited mixing.[79] These limitations can be overcome through the design of a branched microfluidic network in which a buffer and a (fluorescently labeled) solution, for which the concentration gradient will be established, are injected through separate channels that split and recombine; the hydraulic resistance of the branches and the number of buffer or solution inlets can be tuned. The final concentration gradient, which is measured across the width of the outlet channel of the device and quantified by the fluorescence intensity, can have Gaussian, skew, exponential, and power-law forms.[80,81] Nonlinear gradient makers can also be designed by placing barriers of different lengths and in varied numbers, aligned with the direction of fluid flow, to separate and guide streams of flowing solutions in a channel.[79]

6.3. Nonlinear Flows in Devices with Geometric Barriers

Nonlinearities in microfluidic flows can occur in devices with geometric barriers. When placed at the opening of a converging channel, a cylindrical barrier can suppress[82] the breakup of droplets in a dense packing of flowing droplets.[83] Droplets are forced to travel through the narrow gaps demarcated by the barrier and the converging nozzle. Due to the velocity differential between the front and back ends of a droplet as it emerges from the gap, it elongates in the direction perpendicular to the flow, which counteracts the elongation in the streamwise direction that leads to breakup.[82]

Particles can also be separated by size when flowing through a microfluidic channel containing an array of cylindrical posts. The array consists of rows of cylinders that are evenly spaced by a distance λ. Each row of cylinders is laterally offset by $\Delta\lambda$ relative to the one above, where $\Delta\lambda$ is a fraction of λ. Size separation of the particles occurs because ones that are smaller in diameter than λ will follow the fluid streamlines, while ones that are larger than λ will bump into the posts and follow the streamlines that coincide with their center of mass. The collision of the large particles with the posts leads to nonlinearities in their motion—dependent on the particle size and not collinear with the pressure gradient. To separate particles with more than two sizes, the array of posts can be extended such that it is composed of multiple sections, each with a unique post diameter, without changing the values of λ and $\Delta\lambda$ between sections.[84]

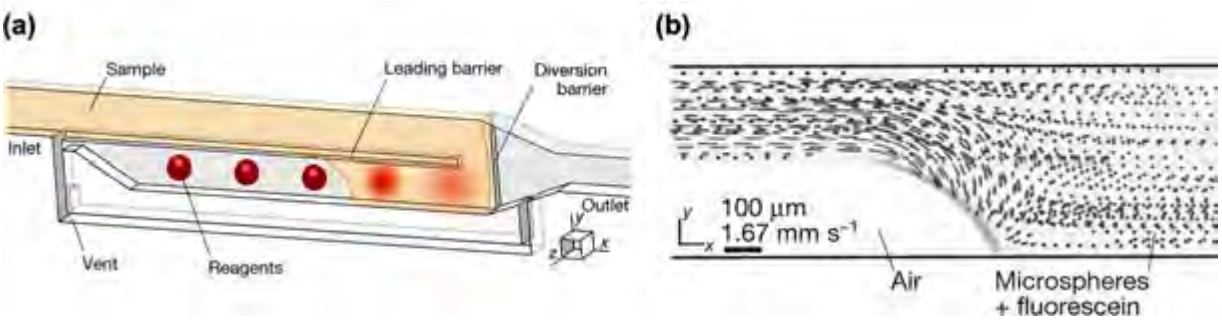

Figure 8. (a) Self-coalescence module in which a fluid (in yellow) mixes with a dried reagent (in red) that is spotted on a substrate due to the presence of a shallow leading barrier that functions as a capillary pinning line. (b) Long-exposure images of 4.8 μm tracer particles inside the module, where the leading barrier is not pictured due to background subtraction. Figure adapted from 89. Copyright 2019 Springer Nature.

https://doi.org/10.1021/acs.chemrev.1c00985
Chem. Rev. 2022, 122, 6921−6937

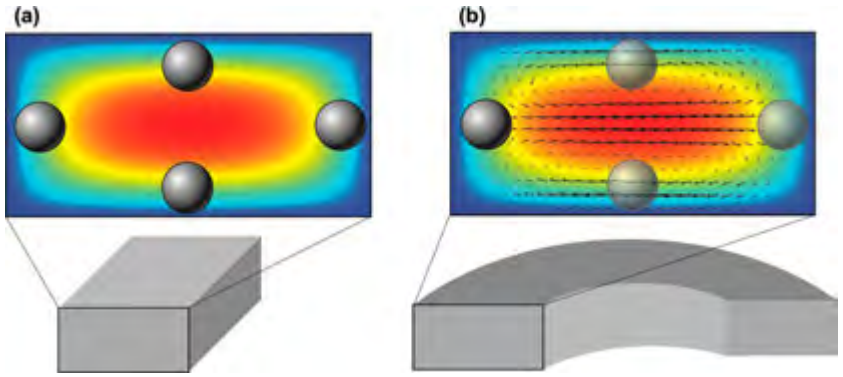

Figure 9. Cross-sectional view of the fluid flow velocity profile within (a) a straight rectangular channel and (b) a curved rectangular channel at intermediate Reynolds numbers, where the velocity ranges from zero (in dark blue) at the walls to its highest value (in red) at the center. When the flowing liquid contains particles, the particles in the straight channel are focused into equilibrium positions, which are marked by gray circles in panel (a) for a specific set of experimental conditions. When the channel is curved, some equilibrium positions become unstable, as indicated by the translucent gray circles in panel (b) for this set of conditions. The arrows in panel (b) show the secondary Dean vortices that emerge. Flow patterns reproduced from 93. Copyright 2014 Annual Reviews Inc.

6.4. Capillary-Driven Flows

Capillary-driven flows in microfluidic channels can occur spontaneously and in the absence of pressure gradients. Examples include liquid wicking through the pores of dry paper[85] and fluid flowing through *open* or *suspended* channels with neither tops nor bottoms.[86] In the former case, the distance that the liquid has advanced, as measured from its point of injection, scales with the square root of time.[87] In the latter case, the fluid advances through a channel filled with air or an immiscible liquid to reduce its total interfacial energy.[86]

Capillary forces can also be used to mix a dried reagent, spotted on a substrate, and a liquid. Normally, Taylor−Aris dispersion causes a reagent to accumulate at the front of a flowing liquid plug, which results in a concentration gradient of the reconstituted reagent.[88] In a microfluidic channel, a narrow barrier, located between an air-filled compartment in which dried reagents are spotted on a substrate and a compartment containing a flowing liquid, causes the liquid to flow back on itself rather than proceed longitudinally, as per Figure 8a. The barrier serves as a capillary pinning line such that the fluid flows toward the liquid−gas interface, as evidenced by Figure 8b.[89] This promotes mixing between the liquid and the spotted reagents before the well-mixed solution bursts past a valve,[90] or *diversion barrier*, and into the rest of the device. The concentration profile of the reconstituted reagents can be controlled by tuning the size of and spacing between the spots.[89]

8.5. Inertial Microfluidics

Inertial microfluidics refers to inertial flows that arise in, for example, curved microfluidic channels or devices operated at intermediate Reynolds numbers. For a curved channel whose cross-sectional radius, w, is far less than its radius of curvature, R, the characteristic axial flow velocity, u, can be approximated by the familiar parabolic flow in a pipe given by eq 6:

$$u \sim u_0[1 - (r/w)^2] \tag{6}$$

where u_0 is the magnitude of the velocity along the centerline of the channel and r is the radial distance from the centerline such that $u = 0$ at the walls as per the no-slip boundary condition. The inertial centrifugal force per unit volume of fluid, f_{inertial}, cannot be neglected; rather, it can be approximated as eq 7:[20]

$$f_{\text{inertial}} \sim \rho {u_0}^2[1 - (r/w)^2]^2/R \tag{7}$$

The variation in the centrifugal force in the radial direction, along with the conservation of mass and the condition of no mass flux across the channel walls, gives rise to two recirculation regions in the channel, above and below the center line of the channel, which are of opposite senses.[20,91] This secondary flow structure is often referred to as a Dean flow, as pictured in Figure 9b. Particles within a fluid flowing in a curved channel will experience a drag force that is proportional to the Dean flow velocity, u_D:

$$u_D \sim \kappa^2 \cdot \mu/2\rho w \tag{8}$$

where $\kappa = Re\sqrt{w/R}$ is the Dean number and $\text{Re} = 2\rho u_0 w/\mu$ is the Reynolds number.[92,91,93] The same analysis extends to tubes with rectangular cross-sections.[94]

At intermediate Reynolds numbers, particles flowing in microfluidic channels migrate to equilibrium positions.[95,96,94] Particle focusing arises due to two predominant inertial lift forces: one that points away from the channel wall and another that points down the shear gradient, which in the case of a pressure-driven Poiseuille flow points from the channel centerline toward the wall.[92,93] The magnitude of the lift force depends on the size of the particles, with radius a, relative to the width of the channel.[92,97] For instance, in the case of particles flowing through a square channel with width H at $\text{Re} = 80$, the lift force, F_{lift}, scales as $F_{\text{lift}} \propto \rho {u_0}^2 a^3/H$ near the channel wall and as $F_{\text{lift}} \propto \rho {u_0}^2 a^6/H^4$ near the channel centerline.[98] When operating a microfluidic device containing curved channels at intermediate Reynolds numbers, equilibrium positions, where particles are inertially focused, may shift relative to their arrangement in non-curved channels at the same Reynolds number,[93] as demonstrated for a specific set of experimental conditions in Figure 9. The ability to manipulate the equilibrium position of particles enables applications in the separation, filtration, or sheath-less alignment of particles.[93,92,97,99,94,100,101]

Oscillations, amplifications, and flow-switching behaviors can be achieved when operating a flow with $\text{Re} \gtrsim O(10)$ in microfluidic channels containing cylindrical posts, as depicted schematically in Figure 10. Braess' paradox, which says that the closure of a channel linking two parallel channels causes an

https://doi.org/10.1021/acs.chemrev.1c00985
Chem. Rev. 2022, 122, 6921−6937

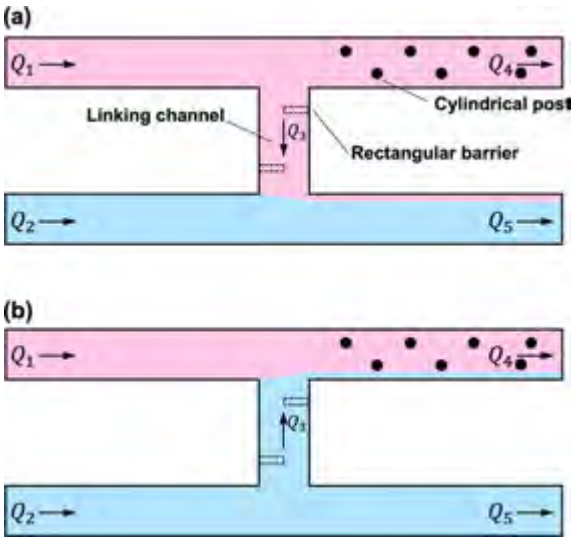

Figure 10. Top-view schematic of a microfluidic device containing cylindrical barriers (solid circles). Two liquids (drawn in pink and in blue) behave according to Braess' paradox, where the total flow rate, as measured by the sum of Q_4 and Q_5, increases upon closing the linking channel. By changing the applied pressure at the inlet, the fluids also exhibit flow-switching behavior where the flow direction in the linking channel changes, as evidenced by panels (a) and (b). The addition of rectangular barriers in the linking channel (dotted-lined rectangles) can lead to further nonlinearities in the flow. Figure inspired by figures appearing in 11 and 12.

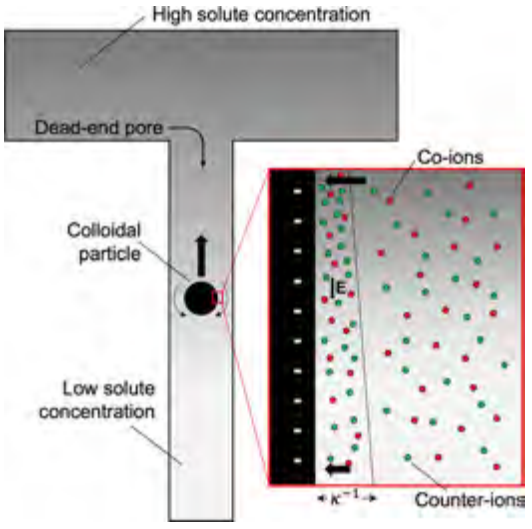

Figure 11. Schematic illustration of the diffusiophoretic migration of a colloidal particle out of a dead-end pore, where dark gray indicates a high concentration level of a binary electrolyte and light gray indicates a low concentration level. As shown in the inset, when suspended in an aqueous solution, the particle acquires a surface charge and the fluid flows along its surface due to an osmotic pressure imbalance within the Debye screening layer (κ^{-1}) and local electrophoresis. The particle moves in the direction opposite to that of the fluid flowing along its surface. Figure inspired by a figure appearing in 133.

increase in the flow throughput,[102] can be reproduced in a microfluidic device at Re $\gtrsim O(10)$ that contains cylindrical obstacles in one of the parallel channels. The direction of flow through the linking channel switches depending on the pressure applied at the inlet of the device. These behaviors can be explained by the Forchheimer effect, whereby the pressure drop across a porous medium (here a channel containing micrometer-sized cylindrical posts) scales quadratically with the flow rate due to non-negligible inertial effects.[11] By simulating the addition of rectangular obstacles in the linking channel, an even greater array of nonlinearities in the flow, including oscillations, bistabilities, conductance switching events, and signal amplification processes, can occur.[12]

6.6. Diffusiophoresis

Diffusiophoresis is a phenomenon by which particles move along solute concentration gradients, which occurs through a combination of chemiphoresis and electrophoresis when the solute is an electrolyte.[103] The former effect refers to the osmotic pressure imbalance along the surface of a particle due to the concentration gradient, which results in the flow of fluid at the particle's surface toward the region of lower solute concentration. The latter effect denotes the flow of fluid within the Debye screening layer of the particle due to the local electric field that arises by virtue of the difference in diffusivities of the co- and counter-ions. Ultimately, the particle moves in the direction opposite to the surface fluid flow. This process is depicted schematically in Figure 11 for a particle with a negative surface charge in the presence of a binary electrolyte whose anion diffuses more quickly than its cation. The diffusiophoretic velocity of a particle scales as the gradient of the logarithm of the solute concentration, meaning that it is a nonlinear function of the solute concentration.[104,105,103] The advent of microfluidic technologies has enabled the creation of sharp concentration gradients at junctions. It has given rise to many possible applications, such as the recovery, filtration, separation, and size segregation of colloidal species, bacteria, and large biomolecules.[104,106,105] Diffusioosmotic effects, which refer to the interaction of the solute with the stationary channel walls, also occur in microfluidic devices.[107]

7. USE OF FLUIDS TO INDUCE NONLINEARITIES IN MICROFLUIDICS

Nonlinear flows can occur in microfluidic devices operated at low Reynolds numbers when special classes of fluids are used, including non-Newtonian fluids[99,3] and liquid metals (mercury and alloys of gallium and indium, such as eutectic gallium indium and Galinstan).[108,109] The Stokes equation (eq 2) cannot accurately describe the flow of non-Newtonian fluids in microfluidics despite the low Reynolds numbers because the stresses in the fluid may be anisotropic and the viscosity may be shear-rate-dependent.[97] Table 2 highlights dimensionless parameters that describe non-Newtonian flows.[20] The Weissenberg number, Wi, is one such parameter, and it corresponds to the ratio of the relaxation time of a polymer in solution to the timescale typical of the extensional or shear flow.[20] When the Weissenberg number is sufficiently high and the Reynolds number is low, namely Re < 1, a non-Newtonian, or viscoelastic, solution composed of a high-molecular-weight polymer in very low volume fractions will effectively undergo turbulent flow. Given the high Weissenberg number, the slow relaxation of the polymer molecules in solution will generate elastic stresses, especially when the flow has curved streamlines. This process is known as *elastic turbulence*.[110] Before the transition to turbulence, the flow undergoes elastic instabilities. In extensional flows, such instabilities occur at Wi $\gtrsim$ 0.5.[111,112]

Elastic turbulence and flow instabilities can be leveraged to expand the functionality of microfluidic devices. First, it is possible to mix two fluids at low Reynolds numbers by adding

https://doi.org/10.1021/acs.chemrev.1c00985
Chem. Rev. 2022, 122, 6921−6937

Table 2. Dimensionless Parameters Describing the Flow of Non-Newtonian Fluids in Microfluidic Devices

Weissenberg number	$\mathrm{Wi} = \tau_p \dot{e}$ or $\mathrm{Wi} = \tau_p \dot{\gamma}$	product of the polymer relaxation time and the deformation rate of the flow
Deborah number	$\mathrm{De} = \frac{\tau_p}{\tau_f}$	ratio of the polymer relaxation time to the characteristic timescale of flow, approximated as $\tau_f = l/u$
elasticity number	$\mathrm{El} = \frac{\mathrm{De}}{\mathrm{Re}} = \frac{\tau_p \mu}{\rho l^2}$	ratio of Deborah to Reynolds numbers or a relative comparison of elastic and inertial effects

where		
	τ_p: characteristic polymer relaxation time	SI units: s
	τ_f: characteristic timescale of flow	SI units: s
	$\dot{e}$: elongational or extensional rate	SI units: s^{-1}
	$\dot{\gamma}$: shear rate	SI units: s^{-1}
	u: characteristic velocity of the fluid	SI units: $m \cdot s^{-1}$
	l: characteristic length scale	SI units: m
	μ: dynamic viscosity of the fluid	SI units: Pa·s
	ρ: density of the fluid	SI units: $kg \cdot m^{-3}$

a high-molecular-weight polymer to the fluids at a concentration as low as tens of parts per million, as shown in Figure 12a. In the absence of the polymer, mixing would be diffusion-limited; however, the introduction of the polymer, coupled with the use of a sinusoidal-shaped planar channel, leads to the mixing of two laminar streams due to elastic stresses in the flow.[113] Second, size-based particle separations can be performed at Reynolds numbers of $O(10^{-4}-10^{-2})$ and Weissenberg numbers of $O(10^{0})$ due to elastic lift forces acting on the flowing particles.[114,115] Particles as small as 20 nm can be effectively separated from a suspension flowing through a rectangular channel with oscillating pressure values across its inlet and outlet.[114] Third, the direction of flow can be rectified. For example, at Wi $\gtrsim$ 0.8, the flow rate of a polymer-containing solution through a planar channel, composed of a sequence of axially aligned triangles whose respective apexes and bases are connected by narrow constrictions, is significantly higher in the forward direction than it is in the reverse direction, as depicted in Figure 12b. This asymmetry occurs because vortices, which emerge at the base corners of each triangle, are more random and irregular in the reverse direction, thereby increasing elastic stresses in the fluid and its resistance to flow.[116] Fourth, upon flowing a polymer solution through a curvy channel that also has contractions and expansions at Wi $\approx$ 1 and Re $\approx$ 0.06, flow rates can be held relatively stable despite changes in applied pressures. Over differential pressures ranging from 22 to 220 Pa, the flow rate through the device only varies by 38%, namely 20 $\pm$ 5 nL·s^{-1}.[117]

Liquid metals, namely metals that are liquid at room temperature, are an emergent class of fluids employed in microfluidic devices. Mercury has been used in micro-electromechanical systems, and its flow can be controlled by applying an electric potential across an electrolyte solution in which it is suspended.[118,119] Now, eutectic gallium indium (EGaIn) and Galinstan, an alloy of gallium, indium, and tin, are choices preferred to liquid mercury due to their low toxicity.[109,108] EGaIn spontaneously forms a thin oxide layer when in contact with air, which means that structures or shapes can be generated that may otherwise be unstable under the influence of gravity or surface tension.[108] The surface tension of an EGaIn−electrolyte solution interface can be reduced by applying a bias voltage to the EGaIn or by chemically removing the oxide layer by treatment with an acid or a base.[120,121] By controlling the bias voltage, the size of EGaIn droplets formed in co-flowing devices[120] or the morphology of EGaIn streams flowing from an orifice into an electrolyte solution[122] can be precisely controlled. Droplets[120] and wires[122] made from liquid metals may contribute to the development of wearable electronics and conductive inks.[123] Other applications of liquid metals in microfluidics[108] range from their use as fugitive inks to print microchannels[124] to their implementation—in droplet form—as fluid mixers owing to Marangoni fluid flows along their surface upon the application of an oscillating bias voltage.[125,126]

8. STIMULI-RESPONSIVE COMPONENTS IN MICROFLUIDICS

It is possible to make geometric components in microfluidic devices from chemically responsive or flexible materials. The structural changes that they undergo may induce nonlinearities in the flow.[20]

8.1. Flexible or Compliant Components

Elastomeric materials can be used as components in microfluidic devices. Their Young's moduli, a material property that

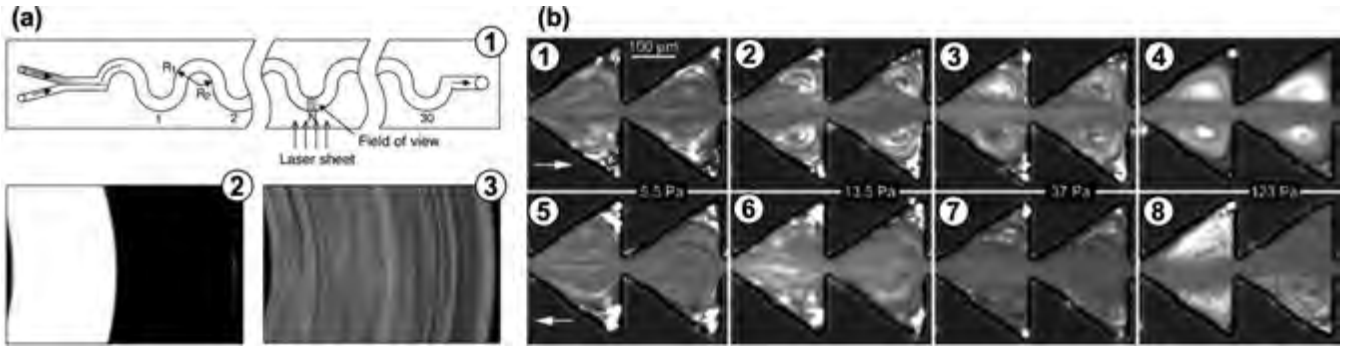

Figure 12. (a) Mixing of two identical aqueous solutions composed of 65% saccharose, 1% sodium chloride, and 80 ppm of polyacrylamide, which are flowed side-by-side in a sinusoidal shaped planar channel at Re = 0.16. The co-flowing streams, one labeled fluorescently which makes it appear white in color, are photographed at the N = 29 half-ring and are well-mixed, as per panel (a3). In the absence of the polymer, the streams do not mix, as shown in panel (a2). (b) Rectification of flow in a microfluidic device upon adding 0.01% by weight of polyacrylamide to an aqueous solution of sucrose, sodium chloride, and Tween 20. Each column corresponds to a given pressure difference across the device. The top row corresponds to flow in the forward direction, and the bottom row corresponds to flow in the reverse direction. Panel (a) adapted from 113. Copyright 2001 Springer Nature. Panel (b) adapted from 116. Copyright 2004 American Physical Society.

https://doi.org/10.1021/acs.chemrev.1c00985
Chem. Rev. 2022, 122, 6921−6937

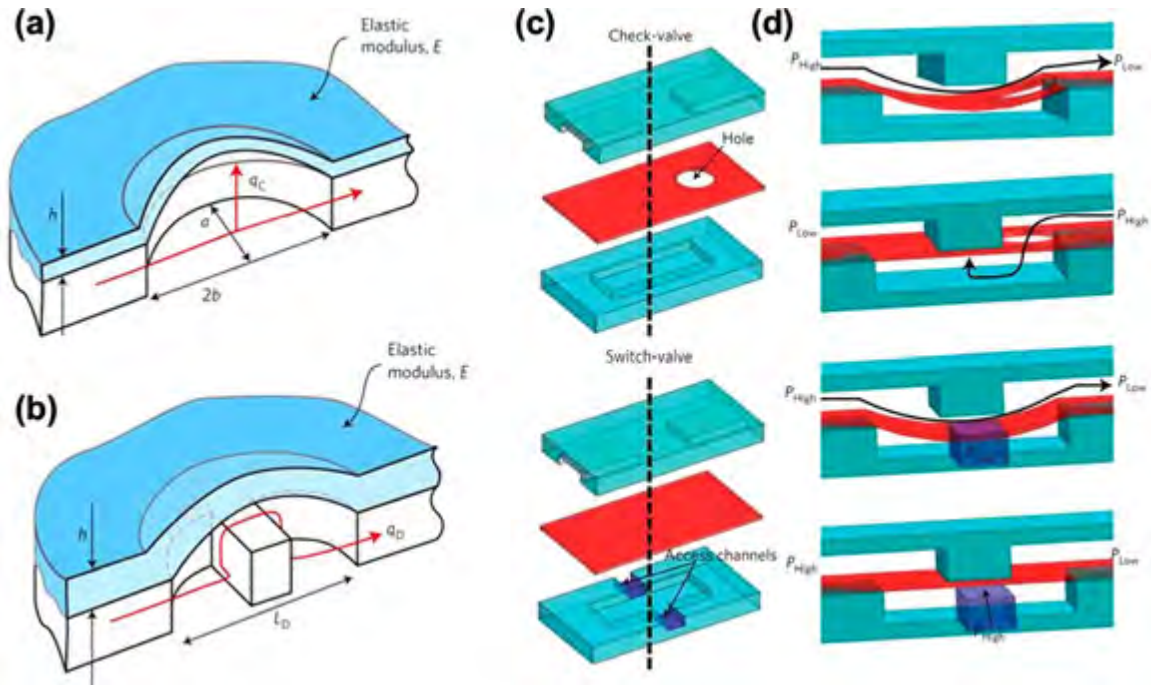

Figure 13. Design of microfluidic (a) capacitors, (b) diodes, and (c and d) check- and switch-valves using flexible elastomeric components. The valves are depicted in both (c) layered and (d) cross-sectional views. Panels (a) and (b) reproduced from 128. Copyright 2009 Springer Nature. Panels (c) and (d) reproduced from 5. Copyright 2010 Springer Nature.

describes their stiffness, can be tailored by altering the relative ratio of the cross-linking agent to the elastomeric base polymer. When the cross-linking agent is present in low amounts, the material is more compliant and, consequently, can experience larger deformations by the flow.[3,127] In fact, compliant elastomers can be cast into membranes that serve as fluidic capacitors, as shown in Figure 13a.[128,129] When the membrane is used to seal the top of a channel, it will expand under flow; its capacitance is defined by the additional volume of fluid that it can accommodate in its deformed state per unit of applied pressure. If a barrier, whose height spans the channel, is introduced, then the component acts as a diode, as illustrated in Figure 13b. When the membrane is undeformed, the fluid flow is obstructed; however, when deflected upward, the fluid can pass through the channel. By actuating a circuit composed of two fluidic branches with an oscillatory pressure input, where each branch contains a capacitor with a distinct resonant frequency (and hence compliance), a resistor, and a diode in series, a band-pass filter is obtained; the flow rate through a particular branch is maximized for a specific excitation frequency. When the oscillatory frequency is sufficiently large, namely $O(10^2-10^3$ Hz), then fluidic inductance must be considered.[128] Here, inductance, L, refers to the inertial effects due to unsteady flows. The pressure change that is induced can be expressed as eq 9:

$$\Delta p_L = L\frac{\mathrm{d}Q}{\mathrm{d}t} \tag{9}$$

where p_L is the pressure change caused by fluid induction and $\mathrm{d}Q/\mathrm{d}t$ is the time derivative of the flow rate Q.[128,3]

Flexible materials can also be used to fabricate flow valves.[3] For example, multi-layer microfluidic devices made from elastomers like polydimethylsiloxane (PDMS), known to many as *Quake valves*,[130] can be used to pump or control the flow of fluids.[130,131] In their simplest iteration, the bottom (or flow) layer contains a network of channels in which fluids flow, while the upper (or control) layer consists of pneumatically activated channels. When a specific channel in the control layer is pressurized, it expands and obstructs—either partially or completely—the flow of fluid through the channel below it. Should a control channel have a rectangular cross-section, then fluid flow may persist when the control channel is pressurized.[130]

Check and switch valves can also be fashioned from multilayer elastomeric components, as per Figures 13(c and d). The valves consist of a flexible membrane that separates two chambers, the top one of which contains a post that contacts the membrane in its undeformed state; each valve admits two fluids as inputs, namely one for each chamber. In the check valve, there is a hole in the membrane. Accordingly, when the membrane is undeformed, the fluids can only flow in one direction, that being through the hole so as to go from the upper chamber to the lower chamber. In the switch valve, a deformable channel is added to the lower chamber. By pressurizing this "access" channel, the membrane can be restored to its undeformed state even when a large pressure gradient is applied across the upper chamber. A microfluidic oscillator can be designed by combining such check and switch valves.[5]

8.2. Chemically Responsive Components

Chemically responsive materials can also be employed in the design of microfluidic devices. These materials can undergo structural changes in response to shifts in pH, temperature, or chemical concentration. Autonomous flow control is made possible by prototyping structures in such deformable materials because the fluid itself induces a structural change in a channel component—for instance, a post or membrane—that may impede its flow.[3] One such example involves coating cylindrical posts with a pH-responsive hydrogel. The hydrogel swells in a basic environment, and eventually the posts become

https://doi.org/10.1021/acs.chemrev.1c00985
Chem. Rev. 2022, 122, 6921−6937

sufficiently wide to block the flow of fluid through a channel; the change in diameter of the posts varies nonlinearly with time and pH.[132] In another example, a hydrogel is employed in the construction of a microfluidic oscillator, which produces an oscillatory flow rate output. In particular, the hydrogel serves as a gating element that swells in the presence of water or aqueous solutions containing low concentrations of alcohol. By introducing water at a constant pressure and alcohol at a constant flow rate as well as extracting fluid from the device at a constant flow rate, it is possible to swell the hydrogel periodically and to obtain an oscillatory flow rate output. When the alcohol injection and fluid extraction flow rates are set to $O(10^1$ uL·min$^{-1})$ and the water pressure is set to $O(10^2$ mbar), the output flow rate oscillates with an approximate frequency of 6 mHz.[4]

9. OUTLOOK AND CONCLUSION

In conclusion, nonlinear phenomena enable new capabilities in microfluidics, especially ones that are atypical of low Reynolds number flows. Bubbles or droplets transform the hydraulic resistances of channels into variable quantities. A bubble or droplet entering a microfluidic network adopts a path that depends on that taken by a bubble or droplet already inside the network; factors like the number of, the spacing between, and the geometric confinement of bubbles or droplets will also affect path selection. Certain bubble and droplet makers can assume various bubbling modes: sometimes they can produce monodisperse bubbles or droplets, and other times they can generate bubbles or droplets in multiple sizes. Remarkably, these behaviors are stable to perturbations. Microfluidic crystals, namely ordered packings of droplets or bubbles in one or two dimension(s), can exhibit vibrational modes, topological rearrangements, and dislocations.

Nonlinearities in single- or two-phase flows can also arise from the geometric features of devices, namely curved channels, when Re > 0 and/or when the flowing fluid is complex. Barriers can be made from inert or stimuli-responsive materials, including compliant elastomers and hydrogels that swell upon changes in the chemical concentration. When a fluid interacts with responsive elements in a microchannel, it can regulate its own flow. For example, the fluid may cause a valve to expand and close, thereby blocking off a channel. At intermediate Reynolds number conditions, particles can be focused to certain positions in microfluidic channels. Furthermore, the flow of non-Newtonian fluids and liquid metals can lead to elastic turbulence or the formation of structures that might otherwise be forbidden by surface tension or gravity.

Nonlinear phenomena in microfluidics, as summarized in Table 3, are undoubtedly worthy of study. They are interesting and defy the common conception of what can be achieved in microfluidics. While the linear and time-reversible characteristics of Stokes flow translate into simpler behaviors in microfluidic devices, nonlinearities extend the capabilities of microfluidic technologies. The discovery of these phenomena can come through the careful observation of experiments conducted in the laboratory, the operation of microfluidic devices in unexplored regimes, and even the design of systems that incorporate materials or concepts uncommon in microfluidics. Although this review has focused almost entirely on experimental realizations of nonlinear phenomena, modeling can be used to predict the emergence of nonlinear behaviors in microfluidic geometries before experimental validation.

Table 3. Summary of Nonlinear Phenomena in Microfluidics and the Source of Their Nonlinearity

phenomenon	source of nonlinearity
bubbles, droplets, and microfluidic crystals	boundary conditions involving interfacial tension
	positions and boundary shapes of bubbles and droplets coupled to those of their neighbors and to the flow
flow of non-Newtonian fluids or liquid metals	rheology of fluids
devices made from stimuli-responsive materials	structural changes in the materials
	boundary conditions dependent on the flow
special topics	
• mixing (namely herringbone mixer)	• spread of dye in a flow is typically a non-linear function of the position of the dye molecules
• capillary-driven flows	• interfacial tension
• diffusiophoresis	• particle velocity is non-linear function of solute concentration

The difficulty that remains is to identify the purpose for which these phenomena can serve. As it stands, nonlinear phenomena are well-suited for study in a curiosity-driven research program. Can they, however, be successfully integrated into technologies for commercial use? There are two challenges in their deployment beyond the laboratory. First, some of their unique characteristics, although hard to come by in other systems, do not lend themselves immediately to practical applications. These include dynamics that are stable to perturbations[55] and the reporting of information pertaining to fluid flow through an entire network at a single junction.[39] Second, the technical implementation of nonlinear microfluidics is not without its challenges. Devices may be made up of many components fashioned from different materials, additives may be required to give fluids non-Newtonian properties, and fluids may be consumed in larger volumes if they are flowed at higher rates. Researchers should strive to make nonlinear microfluidic applications, such as mixing, separations, and fluid gating, more user-friendly; otherwise, these solutions may lose their appeal, namely their portability and microfluidic compatibility, compared to mechanical stirrers, filters, or valves. It is our hope that continued curiosity will lead to the discovery of new phenomena that will expand the microfluidic toolkit and resolve these outstanding challenges.

AUTHOR INFORMATION

Corresponding Authors

Sarah Battat − *John A. Paulson School of Engineering and Applied Sciences, Harvard University, Cambridge, Massachusetts 02138, United States*; Email: sbattat@gmwgroup.harvard.edu

David A. Weitz − *John A. Paulson School of Engineering and Applied Sciences, Harvard University, Cambridge, Massachusetts 02138, United States; Department of Physics, Harvard University, Cambridge, Massachusetts 02138, United States; Wyss Institute for Biologically Inspired Engineering, Harvard University, Boston, Massachusetts 02115, United States;* orcid.org/0000-0001-6678-5208; Email: weitz@seas.harvard.edu

George M. Whitesides − *Department of Chemistry and Chemical Biology, Harvard University, Cambridge, Massachusetts 02138, United States;* orcid.org/0000-

https://doi.org/10.1021/acs.chemrev.1c00985
Chem. Rev. 2022, 122, 6921−6937

0001-9451-2442; Email: gwhitesides@gmwgroup.harvard.edu

Complete contact information is available at: https://pubs.acs.org/10.1021/acs.chemrev.1c00985

Notes

The authors declare no competing financial interest.

Biographies

Sarah Battat received her A.B. degree in Physics and a certificate in Materials Science and Engineering from Princeton University in 2017. She obtained her M.S. in Applied Physics from Harvard University in 2019. She is currently working towards her Ph.D. in Applied Physics under the supervision of George Whitesides and David Weitz. Her research in soft condensed matter physics combines fluid mechanics and self-assembly in dissipative systems.

David A. Weitz received his Ph.D. in Physics from Harvard University and then joined Exxon Research and Engineering Company, where he worked for nearly 18 years. He then became a Professor of Physics at the University of Pennsylvania and moved to Harvard University at the end of the last millennium as Professor of Physics and Applied Physics. He leads a group studying soft matter science with a focus on materials science, biophysics, microfluidics, biotechnology, and flow in porous media. Several start-up companies have come from his lab to commercialize research concepts.

George M. Whitesides received his A.B. degree from Harvard University in 1960 and his Ph.D. from the California Institute of Technology in 1964 (with J. D. Roberts). He began his independent career at M.I.T. and is now the Woodford L. and Ann A. Flowers University Professor at Harvard University. His current research interests include physical and organic chemistry, materials science, biophysics, water, self-assembly, complexity and simplicity, origin of life, dissipative systems, affordable diagnostics, and soft robotics.

ACKNOWLEDGMENTS

Much of what several of us understand about microfluidics we owe to Dr. Howard Stone (Princeton University), who—although not an author of this article—has contributed critically to the education of those who are. We thank him for reading our manuscript and providing important suggestions and guidance. S.B. is supported by the NSF through the Harvard MRSEC award DMR-2011754 and the DARPA award W911NF-18-2-0030. D.A.W. acknowledges support from the NSF through the Harvard MRSEC award DMR-1420570.

REFERENCES

(1) Kirby, B. J. *Micro- and Nanoscale Fluid Mechanics: Transport in Microfluidic Devices*; Cambridge University Press: New York, NY, 2010.
(2) Stone, H. A.; Stroock, A. D.; Ajdari, A. Engingeering Flows in Small Devices: Microfluidics Toward a Lab-on-a-Chip. *Annu. Rev. Fluid Mech.* **2004**, *36*, 381−411.
(3) Xia, H. M.; Wu, J. W.; Zheng, J. J.; Zhang, J.; Wang, Z. P. Nonlinear microfluidics: device physics, functions, and applications. *Lab Chip* **2021**, *21*, 1241−1268.
(4) Paschew, G.; Schreiter, J.; Voigt, A.; Pini, C.; Chávez, J. P.; Allerdißen, M.; Marschner, U.; Siegmund, S.; Schüffny, R.; Jülicher, F.; et al. Autonomous Chemical Oscillator Circuit Based on Bidirectional Chemical-Microfluidic Coupling. *Adv. Mater. Technol.* **2016**, *1*, 1600005.
(5) Mosadegh, B.; Kuo, C.-H.; Tung, Y.-C.; Torisawa, Y.-s.; Bersano-Begey, T.; Tavana, H.; Takayama, S. Integrated elastomeric components for autonomous regulation of sequential and oscillatory flow switching in microfluidic devices. *Nat. Phys.* **2010**, *6*, 433−437.
(6) Fuerstman, M. J.; Garstecki, P.; Whitesides, G. M. Coding/Decoding and Reversibility of Droplet Trains in Microfluidic Networks. *Science.* **2007**, *315*, 828−832.
(7) Anna, S. L. Droplets and Bubbles in Microfluidic Devices. *Annu. Rev. Fluid Mech.* **2016**, *48*, 285−309.
(8) Günther, A.; Jensen, K. F. Multiphase microfluidics: from flow characteristics to chemical and materials synthesis. *Lab Chip.* **2006**, *6*, 1487−1503.
(9) Seo, J.; Lean, M. H.; Kole, A. Membrane-free microfiltration by asymmetric inertial migration. *Appl. Phys. Lett.* **2007**, *91*, 033901.
(10) Shin, S.; Shardt, O.; Warren, P. B.; Stone, H. A. Membraneless water filtration using CO2. *Nat. Commun.* **2017**, *8*, 15181.
(11) Case, D. J.; Liu, Y.; Kiss, I. Z.; Angilella, J.-R.; Motter, A. E. Braess's paradox and programmable behaviour in microfluidic networks. *Nature* **2019**, *574*, 647−652.
(12) Case, D. J.; Angilella, J.-R.; Motter, A. E. Spontaneous oscillations and negative-conductance transitions in microfluidic networks. *Sci. Adv.* **2020**, *6*, aay6761.
(13) Whitesides, G. M. The origins and the future of microfluidics. *Nature.* **2006**, *442*, 368−373.
(14) Seemann, R.; Brinkmann, M.; Pfohl, T.; Herminghaus, S. Droplet based microfluidics. *Rep. Prog. Phys.* **2012**, *75*, 016601.
(15) Shang, L.; Cheng, Y.; Zhao, Y. Emerging Droplet Microfluidics. *Chem. Rev.* **2017**, *117*, 7964−8040.
(16) Baroud, C. N.; Gallaire, F.; Dangla, R. Dynamics of microfluidic droplets. *Lab Chip.* **2010**, *10*, 2032−2045.
(17) Ajaev, V. S.; Homsy, G. M. Modeling Shapes and Dynamic of Confined Bubbles. *Annu. Rev. Fluid Mech.* **2006**, *38*, 277−307.
(18) Tabeling, P. *Introduction to Microfluidics*; Oxford University Press: New York, NY, 2005.
(19) Falkovich, G. *Fluid Mechanics*; Cambridge University Press: Cambridge, U.K., 2018.
(20) Squires, T. M.; Quake, S. R. Microfluidics: Fluid physics at the nanoliter scale. *Rev. Mod. Phys.* **2005**, *77*, 977−1026.
(21) Priest, C.; Herminghaus, S.; Seemann, R. Generation of monodisperse gel emulsions in a microfluidic device. *Appl. Phys. Lett.* **2006**, *88*, 024106.
(22) Li, Z.; Leshansky, A. M.; Pismen, L. M.; Tabeling, P. Step-emulsification in a microfluidic device. *Lab Chip.* **2015**, *15*, 1023−1031.
(23) Montessori, A.; Lauricella, M.; Succi, S.; Stolovicki, E.; Weitz, D. A. Elucidating the mechanism of step emulsification. *Phys. Rev. Fluids.* **2018**, *3*, 072202.
(24) Utada, A. S.; Fernandez-Nieves, A.; Stone, H. A.; Weitz, D. A. Dripping to Jetting Transitions in Coflowing Liquid Streams. *Phys. Rev. Lett.* **2007**, *99*, 094502.
(25) Umbanhowar, P. B.; Prasad, V.; Weitz, D. A. Monodisperse Emulsion Generation via Drop Break Off in a Coflowing Stream. *Langmuir.* **2000**, *16*, 347−351.
(26) Guillot, P.; Colin, A.; Utada, A. S.; Ajdari, A. Stability of a Jet in Confined Pressure-Driven Biphasic Flows at Low Reynolds Numbers. *Phys. Rev. Lett.* **2007**, *99*, 104502.
(27) Wang, K.; Xie, L.; Lu, Y.; Luo, G. Generating microbubbles in a co-flowing microfluidic device. *Chem. Eng. Sci.* **2013**, *100*, 486−495.
(28) Lin, X.; Bao, F.; Tu, C.; Yin, Z.; Gao, X.; Lin, J. Dynamics of bubble formation in highly viscous liquid in co-flowing microfluidic device. *Microfluid. Nanofluidics.* **2019**, *23*, 74.
(29) Garstecki, P.; Gitlin, I.; DiLuzio, W.; Whitesides, G. M.; Kumacheva, E.; Stone, H. A. Formation of monodisperse bubbles in a microfluidic flow-focusing device. *Appl. Phys. Lett.* **2004**, *85*, 2649−2651.
(30) Anna, S. L.; Bontoux, N.; Stone, H. A. Formation of dispersions using "flow focusing" in microchannels. *Appl. Phys. Lett.* **2003**, *82*, 364−366.

(31) Gañán-Calvo, A. M.; Gordillo, J. M. Perfectly Monodisperse Microbubbling by Capillary Flow Focusing. *Phys. Rev. Lett.* **2001**, *87*, 274501.
(32) Garstecki, P.; Fuerstman, M. J.; Stone, H. A.; Whitesides, G. M. Formation of droplets and bubbles in a microfluidic T-junction—scaling and mechanism of break-up. *Lab Chip.* **2006**, *6*, 437−446.
(33) Abate, A. R.; Mary, P.; van Steijn, V.; Weitz, D. A. Experimental validation of plugging during drop formation in a T-junction. *Lab Chip.* **2012**, *12*, 1516−1521.
(34) Thorsen, T.; Roberts, R. W.; Arnold, F. H.; Quake, S. R. Dynamic Pattern Formation in a Vesicle-Generating Microfluidic Device. *Phys. Rev. Lett.* **2001**, *86*, 4163−4166.
(35) Garstecki, P.; Stone, H. A.; Whitesides, G. M. Mechanism for Flow-Rate Controlled Breakup in Confined Geometries: A Route to Monodisperse Emulsions. *Phys. Rev. Lett.* **2005**, *94*, 164501.
(36) Garstecki, P.; Gañán-Calvo, A. M.; Whitesides, G. M. Formation of bubbles and droplets in microfluidic systems. *B. Polym. Acad. Sci.-Technol.* **2005**, *53*, 361−372.
(37) De Menech, M.; Garstecki, P.; Jousse, F.; Stone, H. A. Transition from squeezing to dripping in a microfluidic T-shaped junction. *J. Fluid Mech.* **2008**, *595*, 141−161.
(38) Strutt, J. W. On the Capillary Phenomena of Jets. *Proc. R. Soc. London* **1879**, *29*, 71−97.
(39) Choi, W.; Hashimoto, M.; Ellerbee, A. K.; Chen, X.; Bishop, K. J. M.; Garstecki, P.; Stone, H. A.; Whitesides, G. M. Bubbles navigating through networks of microchannels. *Lab Chip.* **2011**, *11*, 3970−3978.
(40) Belloul, M.; Engl, W.; Colin, A.; Panizza, P.; Ajdari, A. Competition between Local Collisions and Collective Hydrodynamic Feedback Controls Traffic Flows in Microfluidic Networks. *Phys. Rev. Lett.* **2009**, *102*, 194502.
(41) Mandal, J.; Sarkar, S.; Sen, S. A deterministic model for bubble propagation through simple and cascaded loops of microchannels in power-law fluids. *Phys. Fluids.* **2021**, *33*, 072008.
(42) Schindler, M.; Ajdari, A. A Droplet Traffic in Microfluidic Networks: A Simple Model for Understanding and Designing. *Phys. Rev. Lett.* **2008**, *100*, 044501.
(43) Maddala, J.; Vanapalli, S. A.; Rengaswamy, R. Origin of periodic and chaotic dynamics due to drops moving in a microfluidic loop device. *Phys. Rev. E* **2014**, *89*, 023015.
(44) Prakash, M.; Gershenfeld, N. Microfluidic Bubble Logic. *Science* **2007**, *315*, 832−835.
(45) Ahn, B.; Lee, K.; Lee, H.; Panchapakesan, R.; Oh, K. W. Parallel synchronization of two trains of droplets using a railroad-like channel network. *Lab Chip.* **2011**, *11*, 3956−3962.
(46) Fuerstman, M. J.; Lai, A.; Thurlow, M. E.; Shevkoplyas, S. S.; Stone, H. A.; Whitesides, G. M. The pressure drop along rectangular microchannels containing bubbles. *Lab Chip.* **2007**, *7*, 1479−1489.
(47) Amon, A.; Schmit, A.; Salkin, L.; Courbin, L.; Panizza, P. Path selection rules for droplet trains in single-lane microfluidic networks. *Phys. Rev. E* **2013**, *88*, 013012.
(48) Engl, W.; Roche, M.; Colin, A.; Panizza, P.; Ajdari, A. Droplet Traffic at a Simple Junction at Low Capillary Numbers. *Phys. Rev. Lett.* **2005**, *95*, 208304.
(49) Cybulski, O.; Garstecki, P.; Grzybowski, B. A. Oscillating droplet trains in microfluidic networks and their suppression in blood flow. *Nat. Phys.* **2019**, *15*, 706−713.
(50) Zhang, Q.; Gheres, K. W.; Drew, P. J. Origins of 1/f-like tissue oxygenation fluctuations in the murine cortex. *PLOS Biol.* **2021**, *19*, e3001298.
(51) Podgoreanu, M. V.; Stout, R. G.; El-Moalem, H.; Silverman, D. G. Synchronous Rhythmical Vasomotion in the Human Cutaneous Microvasculature during Nonpulsatile Cardiopulmonary Bypass. *Anesthesiology.* **2002**, *97*, 1110−1117.
(52) Kiani, M. F.; Pries, A. R.; Hsu, L. L.; Sarelius, I. H.; Cokelet, G. R. Fluctuations in microvascular blood flow parameters caused by hemodynamic mechanisms. *Am. J. Physiol. Heart Circ. Physiol.* **1994**, *266*, H1822−H1828.
(53) Dreyfus, R.; Tabeling, P.; Willaime, H. Ordered and Disordered Patterns in Two-Phase Flows. *Phys. Rev. Lett.* **2003**, *90*, 144505.
(54) Hashimoto, M.; Garstecki, P.; Whitesides, G. M. Synthesis of Composite Emulsions and Complex Foams with the use of Microfluidic Flow-Focusing Devices. *Small.* **2007**, *3*, 1792−1802.
(55) Garstecki, P.; Fuerstman, M. J.; Whitesides, G. M. Oscillations with uniquely long periods in a microfluidic bubble generator. *Nat. Phys.* **2005**, *1*, 168−171.
(56) Garstecki, P.; Fuerstman, M. J.; Whitesides, G. M. Nonlinear Dynamics of a Flow-Focusing Bubble Generator: An Inverted Dripping Faucet. *Phys. Rev. Lett.* **2005**, *94*, 234502.
(57) Hashimoto, M.; Shevkoplyas, S. S.; Zasońska, B.; Szymborski, T.; Garstecki, P.; Whitesides, G. M. Formation of Bubbles and Droplets in Parallel, Coupled Flow-Focusing Geometries. *Small.* **2008**, *4*, 1795−1805.
(58) Beatus, T.; Tlusty, T.; Bar-Ziv, R. Phonons in a one-dimensional microfluidic crystal. *Nat. Phys.* **2006**, *2*, 743−748.
(59) Beatus, T.; Bar-Ziv, R. H.; Tlusty, T. The physics of 2D microfluidic droplet ensembles. *Phys. Rep.* **2012**, *516*, 103−145.
(60) Beatus, T.; Bar-Ziv, R.; Tlusty, T. Anomalous Microfluidic Phonons Induced by the Interplay of Hydrodynamic Screening and Incompressibility. *Phys. Rev. Lett.* **2007**, *99*, 124502.
(61) Shani, I.; Beatus, T.; Bar-Ziv, R. H.; Tlusty, T. Long-range orientational order in two-dimensional microfluidic dipoles. *Nat. Phys.* **2014**, *10*, 140−144.
(62) Beatus, T.; Tlusty, T.; Bar-Ziv, R. Burgers Shock Waves and Sound in a 2D Microfluidic Droplets Ensemble. *Phys. Rev. Lett.* **2009**, *103*, 114502.
(63) Del Giudice, F.; D'Avino, G.; Maffettone, P. L. Microfluidic formation of crystal-like structures. *Lab Chip.* **2021**, *21*, 2069−2094.
(64) Claussen, O.; Herminghaus, S.; Brinkmann, M. Packings of monodisperse emulsions in flat microfluidic channels. *Phys. Rev. E* **2012**, *85*, 061403.
(65) Hashimoto, M.; Mayers, B.; Garstecki, P.; Whitesides, G. M. Flowing Lattices of Bubbles as Tunable, Self-Assembled Diffraction Gratings. *Small.* **2006**, *2*, 1292−1298.
(66) Garstecki, P.; Whitesides, G. M. Flowing Crystals: Non-equilibrium Structure of Foam. *Phys. Rev. Lett.* **2006**, *97*, 024503.
(67) Raven, J.-P.; Marmottant, P. Microfluidic Crystals: Dynamic Interplay between Rearrangement Waves and Flow. *Phys. Rev. Lett.* **2009**, *102*, 084501.
(68) Montessori, A.; Lauricella, M.; Tiribocchi, A.; Succi, S. Modeling pattern formation in soft flowing crystals. *Phys. Rev. Fluids.* **2019**, *4*, 072201.
(69) Huerre, A.; Miralles, V.; Jullien, M.-C. Bubbles and foams in microfluidics. *Soft Matter.* **2014**, *10*, 6888−6902.
(70) Gai, Y.; Leong, C. M.; Cai, W.; Tang, S. K. Y. Spatiotemporal periodicity of dislocation dynamics in a two-dimensional microfluidic crystal flowing in a tapered channel. *Proc. Natl. Acad. Sci. U.S.A.* **2016**, *113*, 12082−12087.
(71) Gai, Y.; Bick, A.; Tang, S. K. Y. Timescale and spatial distribution of local plastic events in a two-dimensional microfluidic crystal. *Phys. Rev. Fluids.* **2019**, *4*, 014201.
(72) Vecchiolla, D.; Biswal, S. L. Dislocation mechanisms in the plastic deformation of monodisperse wet foams within an expansion-contraction microfluidic geometry. *Soft Matter.* **2019**, *15*, 6207−6223.
(73) Stroock, A. D.; Dertinger, S. K. W.; Ajdari, A.; Mezić, I.; Stone, H. A.; Whitesides, G. M. Chaotic Mixer for Microchannels. *Science.* **2002**, *295*, 647−651.
(74) Lee, C.-Y.; Chang, C.-L.; Wang, Y.-N.; Fu, L.-M. Microfluidic Mixing: A Review. *Int. J. Mol. Sci.* **2011**, *12*, 3263−3287.
(75) Ward, K.; Fan, Z. H. Mixing in microfluidic devices and enhancement methods. *J. Micromech. Microeng.* **2015**, *25*, 094001.
(76) Tabeling, P.; Chabert, M.; Dodge, A.; Jullien, C.; Okkels, F. Chaotic Mixing in Cross-Channel Micromixers. *Philos. Trans. Math. Phys. Eng. Sci.* **2004**, *362*, 987−1000.
(77) Garstecki, P.; Fuerstman, M. J.; Fischbach, M. A.; Sia, S. K.; Whitesides, G. M. Mixing with bubbles: A practical technology for use with portable microfluidic devices. *Lab Chip.* **2006**, *6*, 207−212.

https://doi.org/10.1021/acs.chemrev.1c00985
Chem. Rev. 2022, 122, 6921−6937

(78) Song, H.; Tice, J. D.; Ismagilov, R. F. A Microfluidic System for Controlling Reaction Networks in Time. *Angew. Chem., Int. Ed.* **2003**, *42*, 768−772.
(79) Irimia, D.; Geba, D. A.; Toner, M. Universal Microfluidic Gradient. *Anal. Chem.* **2006**, *78*, 3472−3477.
(80) Jeon, N. L.; Dertinger, S. K. W.; Chiu, D. T.; Choi, I. S.; Stroock, A. D.; Whitesides, G. M. Generation of Solution and Surface Gradients Using Microfluidic Systems. *Lamgmuir.* **2000**, *16*, 8311−8316.
(81) Lin, F.; Saadi, W.; Rhee, S. W.; Wang, S.-J.; Mittal, S.; Jeon, N. L. Generation of dynamic temporal and spatial concentration gradients using microfluidic devices. *Lab Chip.* **2004**, *4*, 164−167.
(82) Bick, A. D.; Khor, J. W.; Gai, Y.; Tang, S. K. Y. Strategic placement of an obstacle suppresses droplet break up in the hopper flow of a microfluidic crystal. *Proc. Natl. Acad. Sci. U.S.A.* **2021**, *118*, e2017822118.
(83) Rosenfeld, L.; Fan, L.; Chen, Y.; Swoboda, R.; Tang, S. K. Y. Break-up of droplets in a concentrated emulsion flowing through a narrow constriction. *Soft Matter.* **2014**, *10*, 421−430.
(84) Huang, L. R.; Cox, E. C.; Austin, R. H.; Sturm, J. C. Continuous Particle Separation Through Deterministic Lateral Displacement. *Science.* **2004**, *304*, 987−990.
(85) Martinez, A. W.; Phillips, S. T.; Butte, M. J.; Whitesides, G. M. Patterned Paper as a Platform for Inexpensive, Low-Volume, Portable Bioassays. *Angew. Chem., Int. Ed.* **2007**, *46*, 1318−1320.
(86) Casavant, B. P.; Berthier, E.; Theberge, A. B.; Berthier, J.; Montanez-Sauri, S. I.; Bischel, L. L.; Brakke, K.; Hedman, C. J.; Bushman, W.; Keller, N. P.; et al. Suspended microfluidics. *Proc. Natl. Acad. Sci. U.S.A.* **2013**, *110*, 10111−10116.
(87) Carrilho, E.; Martinez, A. W.; Whitesides, G. M. Understanding Wax Printing: A Simple Micropatterning Process for Paper-Based Microfluidics. *Anal. Chem.* **2009**, *81*, 7091−7095.
(88) Taylor, G. I. Dispersion of Soluble Matter in Solvent Flowing Slowly through a Tube. *Proc. R. Soc. London A Math. Phys. Sci.* **1953**, *219*, 186−203.
(89) Gökçe, O.; Castonguay, S.; Temiz, Y.; Gervais, T.; Delamarche, E. Self-coalescing flows in microfluidics for pulse-shaped delivery of reagents. *Nature.* **2019**, *574*, 228−232.
(90) Safavieh, R.; Juncker, D. Capillarics: pre-programmed, self-powered microfluidic circuits built from capillary elements. *Lab Chip.* **2013**, *13*, 4180−4189.
(91) Berger, S. A.; Talbot, L.; Yao, L.-S. Flow in Curved Pipes. *Annu. Rev. Fluid Mech.* **1983**, *15*, 461−512.
(92) Di Carlo, D. Inertial microfluidics. *Lab Chip.* **2009**, *9*, 3038−3046.
(93) Martel, J. M.; Toner, M. Inertial Focusing in Microfluidics. *Annu. Rev. Biomed. Eng.* **2014**, *16*, 371−396.
(94) Di Carlo, D.; Irimia, D.; Tompkins, R. G.; Toner, M. Continuous inertial focusing, ordering, and separation of particles in microchannels. *Proc. Natl. Acad. Sci. U.S.A.* **2007**, *104*, 18892−18897.
(95) Segré, G.; Silberberg, A. Behaviour of macroscopic rigid spheres in Poiseuille flow Part 2. Experimental results and interpretation. *J. Fluid Mech.* **1962**, *14*, 136−157.
(96) Matas, J.-P.; Morris, J. F.; Guazzelli, É. Inertial migration of rigid spherical particles in Poiseuille flow. *J. Fluid Mech.* **1999**, *515*, 171−195.
(97) Stoecklein, D.; Di Carlo, D. Nonlinear Microfluidics. *Anal. Chem.* **2019**, *91*, 296−314.
(98) Di Carlo, D.; Edd, J. F.; Humphry, K. J.; Stone, H. A.; Toner, M. Particle Segregation and Dynamics in Confined Flows. *Phys. Rev. Lett.* **2009**, *102*, 094503.
(99) Amini, H.; Lee, W.; Di Carlo, D. Inertial microfluidic physics. *Lab Chip.* **2014**, *14*, 2739−2761.
(100) Di Carlo, D.; Edd, J. F.; Irimia, D.; Tompkins, R. G.; Toner, M. Equilibrium Separation and Filtration of Particles Using Differential Inertial Focusing. *Anal. Chem.* **2008**, *80*, 2204−2211.
(101) Seo, J.; Lean, M. H.; Kole, A. Membrane-free microfiltration by asymmetric inertial migration. *Appl. Phys. Lett.* **2007**, *91*, 033901.
(102) Braess, D.; Nagurney, A.; Wakolbinger, T. On a Paradox of Traffic Planning. *Transp. Sci.* **2005**, *39*, 446−450.
(103) Prieve, D. C.; Anderson, J. L.; Ebel, J. P.; Lowell, M. E. Motion of a particle generated by chemical gradients. Part 2. Electrolytes. *J. Fluid Mech.* **1984**, *148*, 247−269.
(104) Velegol, D.; Garg, A.; Guha, R.; Kar, A.; Kumar, M. Origins of concentration gradients for diffusiophoresis. *Soft Matter.* **2016**, *12*, 4686−4703.
(105) Shin, S. Diffusiophoretic separation of colloids in microfluidic flows. *Phys. Fluids.* **2020**, *32*, 101302.
(106) Kar, A.; Chiang, T.-Y.; Ortiz Rivera, I.; Sen, A.; Velegol, D. Enhanced Transport into and out of Dead-End Pores. *ACS Nano* **2015**, *9*, 746−753.
(107) Marbach, S.; Bocquet, L. Osmosis, from molecular insights to large-scale applications. *Chem. Soc. Rev.* **2019**, *48*, 3102−3144.
(108) Khoshmanesh, K.; Tang, S.-Y.; Zhu, J. Y.; Schaefer, S.; Mitchell, A.; Kalantar-Zadeh, K.; Dickey, M. D. Liquid metal enable microfluidics. *Lab Chip.* **2017**, *17*, 974−993.
(109) Dickey, M. D.; Chiechi, R. C.; Larsen, R. J.; Weiss, E. A.; Weitz, D. A.; Whitesides, G. M. Eutectic Gallium-Indium (EGaIn): A Liquid Metal Alloy for the Formation of Stable Structures in Microchannels at Room Temperature. *Adv. Funct. Mater.* **2008**, *18*, 1097−1104.
(110) Groisman, A.; Steinberg, V. Elastic turbulence in a polymer solution flow. *Nature.* **2000**, *405*, 53−55.
(111) Sousa, P.; Pinho, F. T.; Alves, M. A. Purely-elastic flow instabilities and elastic turbulence in microfluidic cross-slot devices. *Soft Matter.* **2018**, *14*, 1344−1354.
(112) Pakdel, P.; McKinley, G. H. Elastic Instability and Curved Streamlines. *Phys. Rev. Lett.* **1996**, *77*, 2459−2462.
(113) Groisman, A.; Steinberg, V. Efficient mixing at low Reynolds numbers using polymer additives. *Nature.* **2001**, *410*, 905−908.
(114) Asghari, M.; Cao, X.; Mateescu, B.; van Leeuwen, D.; Aslan, M. K.; Stavrakis, S.; deMello, A. J. Oscillatory Viscoelastic Microfluidics for Efficient Focusing and Separation of Nanoscale Species. *ACS Nano* **2020**, *14*, 422−433.
(115) Romeo, G.; D'Avino, G.; Greco, F.; Netti, P. A.; Maffettone, P. L. Viscoelastic flow-focusing in microchannels: scaling, properties of the particle radial distributions. *Lab Chip.* **2013**, *13*, 2802−2807.
(116) Groisman, A.; Quake, S. R. A Microfluidic Rectifier: Anisotropic Flow Resistance at Low Reynolds Numbers. *Phys. Rev. Lett.* **2004**, *92*, 094501.
(117) Groisman, A.; Enzelberger, M.; Quake, S. R. Microfluidic Memory and Control Devices. *Science.* **2003**, *300*, 955−958.
(118) Lee, J.; Kim, C.-J. Surface-Tension-Driven Microactuation Based on Continuous Electrowetting. *J. Microelectromech. Syst.* **2000**, *9*, 171−180.
(119) Yun, K.-S.; Cho, I.-J.; Bu, J.-U.; Kim, C.-J.; Yoon, E. A Surface-Tension Driven Micropump for Low-Voltage and Low-Power Operations. *J. Microelectromech. Syst.* **2002**, *11*, 454−461.
(120) Tang, S.-Y.; Joshipura, I. D.; Lin, Y.; Kalantar-Zadeh, K.; Mitchell, A.; Khoshmanesh, K.; Dickey, M. D. Liquid-Metal Microdroplets Formed Dynamically with Electrical Control of Size and Rate. *Adv. Mater.* **2016**, *28*, 604−609.
(121) Khan, M. R.; Trlica, C.; Dickey, M. D. Recapillarity: Electrochemically Controlled Capillary Withdrawal of a Liquid Metal Alloy from Microchannels. *Adv. Funct. Mater.* **2015**, *25*, 671−678.
(122) Song, M.; Kartawira, K.; Hillaire, K. D.; Li, C.; Eaker, C. B.; Kiani, A.; Daniels, K. E.; Dickey, M. D. Overcoming Rayleigh-Plateau instabilities: Stabilizing and destabilizing liquid-metal streams via electrochemical oxidation. *Proc. Natl. Acad. Sci. U.S.A.* **2020**, *117*, 19026−19032.
(123) Zhu, L.; Wang, B.; Handschuh-Wang, S.; Zhou, X. Liquid Metal-Based Soft Microfluidics. *Small.* **2020**, *16*, 1903841.
(124) Parekh, D. P.; Ladd, C.; Panich, L.; Moussa, K.; Dickey, M. D. 3D printing of liquid metals as fugitive inks for fabrication of 3D microfluidic channels. *Lab Chip.* **2016**, *16*, 1812−1820.

https://doi.org/10.1021/acs.chemrev.1c00985
Chem. Rev. 2022, 122, 6921−6937

(125) Tang, S.-Y.; Khoshmanesh, K.; Sivan, V.; Petersen, P.; O'Mullane, A. P.; Abbott, D.; Mitchell, A.; Kalantar-Zadeh, K. Liquid metal enabled pump. *Proc. Natl. Acad. Sci. U.S.A.* **2014**, *111*, 3304−3309.
(126) Tang, S.-Y.; Sivan, V.; Petersen, P.; Zhang, W.; Morrison, P. D.; Kalantar-Zadeh, K.; Mitchell, A.; Khoshmanesh, K. Liquid Metal Actuator for Inducing Chaotic Advection. *Adv. Funct. Mater.* **2014**, *24*, 5851−5858.
(127) Quake, S. R.; Scherer, A. From Micro-to Nanofabrication with Soft Materials. *Science.* **2000**, *290*, 1536−1540.
(128) Leslie, D. C.; Easley, C. J.; Seker, E.; Karlinsey, J. M.; Utz, M.; Begley, M. R.; Landers, J. P. Frequency-specific flow control in microfluidic circuits with passive elastomeric features. *Nat. Phys.* **2009**, *5*, 231−235.
(129) Kim, S.-J.; Yokokawa, R.; Takayama, S. Microfluidic oscillators with widely tunable periods. *Lab Chip.* **2013**, *13*, 1644−1648.
(130) Unger, M. A.; Chou, H.-P.; Thorsen, T.; Scherer, A.; Quake, S. R. Monolithic Microfabricated Valves and Pumps by Multilayer Soft Lithography. *Science.* **2000**, *288*, 113−116.
(131) Thorsen, T.; Maerkl, S. J.; Quake, S. R. Microfluidic Large-Scale Integration. *Science.* **2002**, *298*, 580−584.
(132) Beebe, D. J.; Moore, J. S.; Bauer, J. M.; Yu, Q.; Liu, R. H.; Devadoss, C.; Jo, B.-H. Functional hydrogel structures for autonomous flow control inside microfluidic channels. *Nature.* **2000**, *404*, 588−590.
(133) Battat, S. Transport of Colloidal Particles by Diffusiophoresis. Senior Thesis, Princeton University, Princeton, NJ, 2017.

https://doi.org/10.1021/acs.chemrev.1c00985
Chem. Rev. 2022, 122, 6921−6937